Bone Regeneration by Regulated *In Vivo* Gene Transfer Using Biocompatible Polyplex Nanomicelles

Keiji Itaka[1], Shinsuke Ohba[1], Kanjiro Miyata[2], Hiroshi Kawaguchi[3], Kozo Nakamura[3], Tsuyoshi Takato[3], Ung-Il Chung[1] and Kazunori Kataoka[1,2]

[1]*Division of Clinical Biotechnology, Center for Disease Biology and Integrative Medicine, Graduate School of Medicine, The University of Tokyo, Tokyo, Japan;* [2]*Department of Materials Science and Engineering, Graduate School of Engineering, The University of Tokyo, Tokyo, Japan;* [3]*Division of Sensory and Motor System Medicine, Faculty of Medicine, The University of Tokyo, Tokyo, Japan*

Gene therapy is a promising strategy for bone regenerative medicine. Although viral vectors have been intensively studied for delivery of osteogenic factors, the immune response inevitably inhibits bone formation. Thus, safe and efficient non-viral gene delivery systems are in high demand. Toward this end, we developed a polyplex nanomicelle system composed of poly(ethyleneglycol) (PEG)-block-cationer (PEG-b-P[Asp-(DET)]) and plasmid DNA (pDNA). This system showed little cytotoxicity and excellent transfection efficiency to primary cells. By the transfection of constitutively active form of activin receptor-like kinase 6 (caALK6) and runt-related transcription factor 2 (Runx2), the osteogenic differentiation was induced on mouse calvarial cells to a greater extent than when poly(ethylenimine) (PEI) or FuGENE6 were used; this result was due to low cytotoxicity and a sustained gene expression profile. After incorporation into the calcium phosphate cement scaffold, the polyplex nanomicelles were successfully released from the scaffold and transfected surrounding cells. Finally, this system was applied to *in vivo* gene transfer for a bone defect model in a mouse skull bone. By delivering *caALK6* and *Runx2* genes from nanomicelles incorporated into the scaffold, substantial bone formation covering the entire lower surface of the implant was induced with no sign of inflammation at 4 weeks. These results demonstrate the first success in *in vivo* gene transfer with therapeutic potential using polyplex nanomicelles.

Received 31 December 2006; accepted 30 April 2007; published online 5 June 2007. doi:10.1038/sj.mt.6300218

INTRODUCTION

Despite bone's capacity to heal spontaneously, bone repair is not always satisfactory. Approximately 5–10% of fractures do not heal well, resulting in delayed union or non-union with considerable morbidity.[1] Critical bone defects after severe trauma, tumor resection, or revision of total joint arthroplasty remain challenging problems. Autologous bone graft is considered the gold standard technique; however, it has shortcomings concerning both quantity (availability of material) and quality (donor site troubles, graft rejection, disease transmission).[2,3] These problems have heightened the need for bone regenerative medicine that uses tissue engineering techniques.[4]

A promising strategy is to combine adequate scaffolds and signals. Although some scaffolds are osteoconductive, no scaffolds invented so far are known to be osteoinductive,[5] because current scaffold materials cannot activate the signals necessary for osteogenesis. For this purpose, the potential of growth and transcriptional factors has been widely recognized.[6,7] Substantial progress has been made in the basic understanding of major osteogenic signaling molecules such as bone morphogenetic proteins (BMPs),[8] Hedgehogs,[9] Runx2,[10] Wnts,[11] and insulin-like growth factors.[12] In particular, recombinant human BMP-2 and BMP-7 have already been approved by the U.S. Food and Drug Administration for restricted clinical use. However, in spite of the remarkable findings on animal studies, clinical trials using BMP devices have not obtained comparable outcomes.[13,14] Problems such as protein stability, inadequate release profile (initial burst effect), or the need for accessory factors may have caused these inconsistent results.[6,15]

Gene therapy is a promising approach to overcome these problems. Compared with exogenous proteins, which require purification, the gene can express these bioactive factors in the native form at the regeneration site.[6] The sustained synthesis of proteins from the delivered gene can facilitate synchronization between the kinetics of signaling receptor expression and bioactive factor availability.[16] In addition, the combined use of two or more osteoinductive factors to constitute a better osteogenic signal can be evaluated with a high degree of flexibility.[17] For this purpose, viral vectors including adenovirus and adeno-associated virus vectors have been intensively studied for the delivery of the osteoinductive cytokines.[17–21] However, when these viral vectors are used, there is concern about inducing immune responses.[22] Indeed, Egermann *et al.* reported that, after a local injection of BMP-2 expressing adenoviral vector to a bone defect area in sheep, bone formation was significantly reduced even at the untreated contralateral defect area, indicating that the immune

The first two authors contributed equally to this work.

Correspondence: *Kazunori Kataoka, Department of Materials Science and Engineering, Graduate School of Engineering, The University of Tokyo, 7-3-1 Hongo, Bunkyo-ku, Tokyo 113-0033, Japan. E-mail: kataoka@bmw.t.u-tokyo.ac.jp*

response has a systemic inhibitory effect on bone formation after a single injection of adenovirus.[23]

In this context, safe and efficient non-viral gene delivery systems are in high demand. We recently developed a novel polymer-based gene delivery system that showed excellent capacity for *in vitro* transfection.[24] This system is a polyplex nanomicelle composed of poly(ethyleneglycol) (PEG)-block-polycation (PEG-b-P[Asp-(DET)]): PEG-b-polyasparagine carrying the *N*-(2-aminoethyl)aminoethyl group $(CH_2)_2NH(CH_2)_2NH_2$ as the side chain) and plasmid DNA (pDNA). The complexation of block copolymer and pDNA forms a micellar structure, and its characteristics have been found suitable for gene delivery: a diameter of ~100 nm with a PEG palisade enabling complexes to avoid foreign body recognition while providing increased nuclease resistance, increased tolerance under physiologic conditions, and excellent gene expression in a serum-containing medium.[25–27] In addition, the cationic segment of block copolymer was designed to have the buffering capacity of an acidic environment inside the endosomes as effected by the presence of unprotonated amines under neutral pH. By virtue of these features, we effectively transfected genes to culture cells with almost no cytotoxicity.[24]

We undertook the present study to investigate the feasibility of these polyplex nanomicelles for bone regenerative medicine, including the study of: (i) transfection toward various primary cells for the evaluation of efficiency and safety, (ii) induction of osteogenic differentiation by a foreign gene introduction of osteogenic factors, and (iii) *in vivo* gene transfer to a mouse bone defect model to increase the rate of bone regeneration. As will be shown, this system provides sufficient gene expression in a sustained manner both *in vitro* and *in vivo*, and it thus shows a potential therapeutic effect in a bone defect model.

RESULTS

In vitro transfection to human synovial cells

To evaluate the feasibility of polyplex nanomicelles for clinical gene therapy, *in vitro* transfection was performed toward human synovial cells derived from patients suffering from rheumatoid arthritis. By evaluating luciferase gene expression on day 2 of transfection, the polyplex nanomicelles that were formed at an optimal nitrogen/phosphate ratio showed gene expressions comparable to those of linear poly(ethylenimine) (LPEI),[28] which is well known to have excellent transfection efficiency (**Figure 1a**). At the optimal nitrogen/phosphate = 80, the polyplex nanomicelles were observed to have small absolute zeta potentials of around +10 mV (**Supplementary Figure S1**). The nanomicelles maintained appreciable gene expression even on day 5, whereas the gene expression of LPEI showed a marked decrease during the same time frame. To investigate this difference, the cytotoxicity was evaluated by a quantitative assay. Consistent with the results of gene expression, LPEI exhibited prominent cytotoxicity time-dependently (**Figure 1b**). The microscopic images following green fluorescence protein (GFP) gene transfection by LPEI showed apparent morphologic change as well as reduced numbers of cells, whereas the polyplex nanomicelles maintained almost normal phenotype concurrently with GFP expression even on day 5 (**Supplementary Figure S2**). Thus, the polyplex

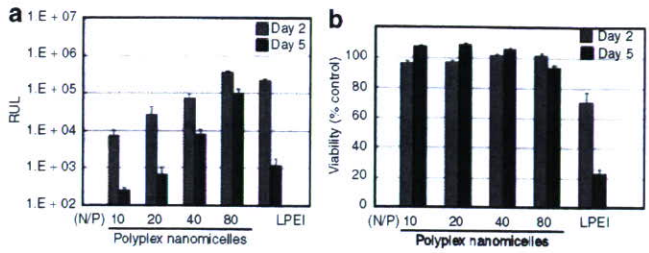

Figure 1 *In vitro* transfection to human synovial cells. (**a**) Luciferase gene expression. *In vitro* transfection of luciferase-expressing plasmid DNA was performed by polyplex nanomicelles formed at various nitrogen/phosphate (N/P) ratios and by poly(ethylenimine) (LPEI). Gene expression was evaluated after 2 and 5 days of transfection. Data are means ± SDs, $n = 4$. (**b**) Cell viability after transfection. After transfection, similar to the case in **a**, cell viability was estimated by an MTT assay. Results were expressed as the relative value (%) of the control cells, which were incubated in parallel without transfection. Data are means ± SDs, $n = 8$. RLU, relative light units.

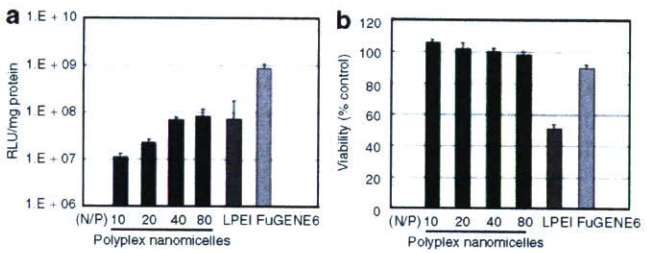

Figure 2 *In vitro* transfection to mouse calvarial cells. (**a**) Luciferase gene expression. *In vitro* transfection of luciferase-expressing plasmid DNA was performed using polyplex nanomicelles, formed at various nitrogen/phosphate (N/P) ratios, as well as poly(ethylenimine) (LPEI) and FuGENE6. Gene expression was evaluated after 2 days of transfection. Data are means ± SDs, $n = 4$. (**b**) Cell viability after transfection. After transfection, similar to the case in **a**, cell viability was estimated by an MTT assay. Results were expressed as relative values (%) of the control cells, which were incubated in parallel without transfection. Data are means ± SDs, $n = 8$. RLU, relative light units.

nanomicelles were revealed to have excellent gene transfection capacity—comparable to that of LPEI—with considerably low cytotoxicity; this suggests a great advantage for *in vivo* application.

Transfection toward mouse calvarial cells and induction of osteogenic differentiation

In applying polyplex nanomicelles to delivery genes encoding bioactive factors that activate signals necessary for osteogenesis, we evaluated the transfection capacity of foreign genes and the induction of cell differentiation toward mouse calvarial cells derived from neonatal calvariae. The evaluation of luciferase showed that gene expressions comparable to those of LPEI were obtained by polyplex nanomicelles (**Figure 2a**) without showing any cytotoxicity (**Figure 2b**). From a practical standpoint we also evaluated FuGENE6, a commercially available lipid-based transfection reagent with considerably high efficiency and biocompatibility.[29–33] With this reagent, the cells showed luciferase expression that was one order higher than with polyplex nanomicelles or LPEI and with little cytotoxicity (**Figure 2a** and **b**).

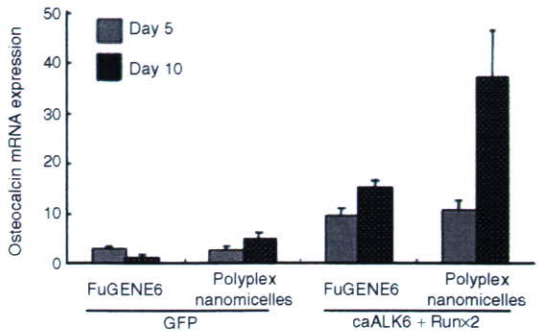

Figure 3 Evaluation of osteocalcin messenger RNA (mRNA) expression by a quantitative polymerase chain reaction (PCR). Osteogenic differentiation was induced on the mouse calvarial cells by transfection of caALK6 and Runx2 expressing plasmid DNAs. As a negative control, a green fluorescence protein (GFP) gene was also used. After 5 and 10 days, the total RNA was collected and the osteocalcin expression was quantified by a quantitative PCR. Data are means ± SDs, $n = 6$. caALK6, constitutively active form of activin receptor-like kinase 6; Runx2, runt-related transcription factor 2.

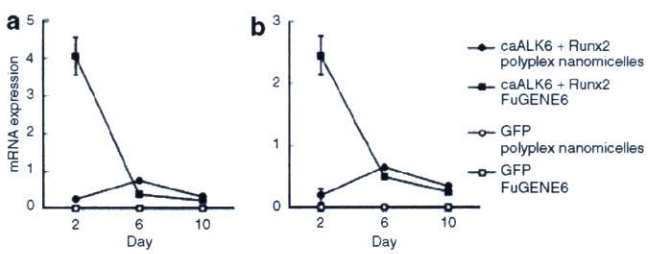

Figure 4 Evaluation of messenger RNA (mRNA) expression of (**a**) constitutively active form of activin receptor-like kinase 6 (caALK6) and (**b**) runt-related transcription factor 2 (Runx2) after transfection by a quantitative polymerase chain reaction. Two, six and ten days after transfection, the mRNA expression of ALK6 and Runx2 was quantified. Data are means ± SDs, $n = 6$. caALK6, constitutively active form of activin receptor-like kinase 6; GFP, green fluorescence protein; Runx2, runt-related transcription factor 2.

Observation of GFP expression revealed that nanomicelles and FuGENE6 achieved similar levels of gene expression without showing any morphologic changes in the cells; this is evident in the phase contrast images (**Supplementary Figure S3**).

We then investigated the osteogenic differentiation after transfection of pDNAs expressing a constitutively active form of activin receptor-like kinase 6 (caALK6) and runt-related transcription factor 2 (Runx2), which have been shown to be a potent combination of genes for bone regeneration.[34] Osteogenic differentiation was evaluated by the expression of osteocalcin messenger RNA (mRNA), an osteoblast-differentiation marker. As shown in **Figure 3**, the time-dependent increase in osteocalcin expression was confirmed after transfection of caALK6 + Runx2 by both polyplex nanomicelles and FuGENE6. Using LPEI, in contrast, osteocalcin expression was at the same level as the control cells transfected with the GFP gene (data not shown). It is interesting that, on day 10, nanomicelles showed a more remarkable increase in osteocalcin expression than did FuGENE6, although both showed comparable gene expression without cytotoxicity by the luciferase and GFP reporter assays (**Figure 2a** and **b** and

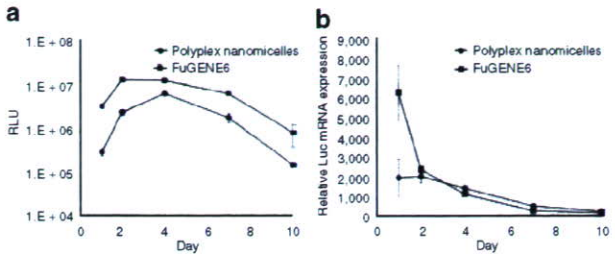

Figure 5 Evaluation of sustained expression of luciferase on mouse calvarial cells. (**a**) Luciferase expression measured by luminescence, which indicated the quantification of protein synthesis. Data are means ± SDs, $n = 12$. (**b**) Estimation of the corresponding messenger RNA (mRNA) expression by a quantitative polymerase chain reaction. For both, the mouse calvarial cells were transfected by luciferase-expressing plasmid DNA and the assays were done on days 1, 2, 4, 7, and 10. Data are means ± SDs, $n = 6$. RLU, relative light units.

Supplementary Figure S3). It is reasonable to assume that, with the same transfection procedure as used with the reporter genes, *caALK6* and *Runx2* were also expressed similarly by nanomicelles and FuGENE6. The reasons for this disparity in osteocalcin induction are unclear, but FuGENE6 may cause some appendant effect on cell differentiation that is difficult to detect by a nonspecific viability evaluation such as the MTT assay.[35] Regarding this concern we speculated that, since the difference was visible on day 10, the expression profile of the transfected genes might differ between nanomicelles and FuGENE6, thus affecting the outcome of the induction of cell differentiation.

To investigate this possibility, the time-dependent change of gene expression was quantified. As shown in **Figure 4**, the mRNA expressions of caALK6 and Runx2 showed similar profiles, where FuGENE6 initially induced expressions of ALK6 and Runx2 that were one order higher than nanomicelles, although the expressions sharply decreased with time. In contrast, the nanomicelles showed rather consistent gene expressions. For a detailed investigation, the luciferase gene was used and the protein systhesis and its mRNA expression were simultaneously quantified by a luminescence measurement and a quantitative polymerase chain reaction (PCR), respectively. As shown in **Figure 5**, FuGENE6 initially showed light emission (indicating the amount of synthesized protein) that was one order higher than did the nanomicelles. The highest expression was obtained on day 2. The initial mRNA expression was always high, but a rapid decrease was observed after day 2. In contrast, the polyplex nanomicelles showed fairly consistent gene expression profiles, giving the highest luciferase expression on day 4 and with sustained mRNA expression thereafter. Because cell differentiation would require some processes in signaling pathways inside the cells, it follows that such a continuous manner of gene expression by polyplex nanomicelles might contribute to the efficient induction of differentiation. Hence, the nanomicelle profile is a promising feature for *in vivo* bone regeneration.

In vitro transfection from gene-containing scaffolds

The *in vivo* gene transfer to a bone regeneration site should require the retention and gradual release of gene carriers. One promising approach is to incorporate the carriers into implantable scaffolds.

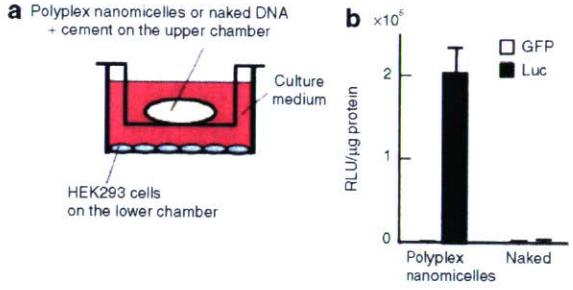

Figure 6 *In vitro* transfection by polyplex nanomicelles incorporated into calcium phosphate cement scaffold. (**a**) Schematic illustration of the *in vitro* transfection from the gene-containing scaffolds. The scaffold containing polyplex nanomicelles of PEG-b-P[Asp-(DET)] and plasmid DNA (pDNA) expressing luciferase gene or naked pDNA was plated onto the upper chamber of cell culture insert, and the HEK293 cells were plated onto the lower chamber. (**b**) Luciferase expression in HEK293 cells. After 5 days of transfection, luciferase expression was measured. The green fluorescence protein (GFP) gene was used as a negative control. Data are means ± SDs, $n = 3$. DET, diethylenetriamine; PEG, poly(ethyleneglycol); RLU, relative light units.

This form of gene delivery is called the gene-activated matrix, through which Bonadio *et al.* pioneered the incorporation of non-viral vectors in collagen scaffolds to stimulate bone formation in a rat defect model.[36] In this study, the polyplex nanomicelles were incorporated into a calcium phosphate cement scaffold by mixing. This process is highly biocompatible, bioactive (especially in bone tissue), moldable, and injectable.

In order to investigate whether or not the polyplex nanomicelles containing luciferase-expressing pDNA were delivered from the calcium phosphate cement scaffold, the scaffold was put into the culture medium of HEK293 cells for 5 days. The cement and the cells were physically separated by a filter to avoid direct contact between the cement and the cells, which could hinder the distinction between the release and the direct delivery of polyplex nanomicelles from the scaffold (**Figure 6**). As shown in **Figure 6b**, the cells cultured with the scaffold containing the polyplex nanomicelles exhibited apparent luciferase expression, whereas the cells cultured with the scaffold containing naked pDNA did not. Thus, the polyplex nanomicelles incorporated into the calcium phosphate cement scaffold successfully introduced the contained genes into the surrounding cells.

Next, to investigate how long the transfection by polyplex nanomicelles incorporated into the scaffold would last, the scaffold was placed on the culture dish and then mouse calvarial cells were plated on top of it and cultured for an extended period. Monitoring of luminescence using the IVIS Imaging System (Xenogen, Alameda, CA) revealed that the gene expression of mouse calvarial cells by the scaffold containing polyplex nanomicelles with luciferase-expressing pDNA increased, peaking near days 10 and 18, and then gradually declined to the background level approaching day 25 (**Supplementary Figure S4a**). Quantitative visualization of luminescence using this imaging system revealed that cells on top of the scaffold and in its close proximity were first transfected at days 2 and 10; subsequently, cells at some distance were transfected until day 25 (**Supplementary Figure S4b**). Thus, the polyplex nanomicelles incorporated into the scaffold delivered genes in a sustained manner.

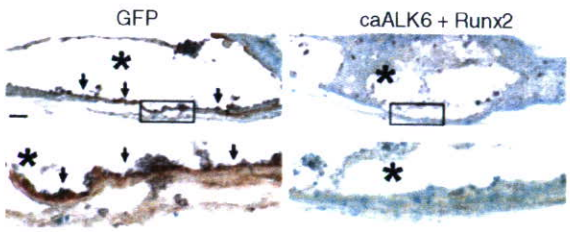

Figure 7 *In vivo* gene transfer by polyplex nanomicelles. Immunohistochemistry for green fluorescence protein (GFP) of calvarias implanted with the scaffold containing polyplex nanomicelles of PEG-b-P[Asp-(DET)] and plasmid DNA expressing GFP or caALK6 + Runx2 at 4 weeks after implantation. GFP protein was stained brown (arrows). The lower panel of each group shows a magnified view of the boxed area in the upper panel. Asterisks denote the remnants of calcium phosphate pastes. Scale bar: 200 μm. caALK6, constitutively active form of activin receptor-like kinase 6; DET, diethylenetriamine; PEG, poly(ethyleneglycol); Runx2, runt-related transcription factor 2.

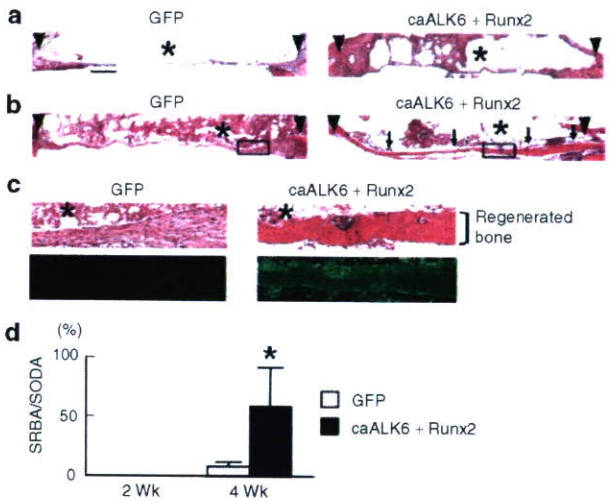

Figure 8 Bone regeneration by polyplex nanomicelles. (**a**, **b**) Histologic analyses of calvarias. The scaffold containing polyplex nanomicelles of PEG-b-P[Asp-(DET)] and plasmid DNA expressing green fluorescence protein (GFP) or caALK6 + Runx2 was implanted on the bone defect area on the mouse skull bone. At (**a**) 2 weeks and (**b**) 4 weeks after implantation, histologic and immunohistologic analyses were performed. Sections were stained with hematoxylin and eosin (H&E). Arrowheads denote defect edges; arrows, regenerated bones; asterisks, the remnants of calcium phosphate cement. Scale bar: 500 μm. (**c**) Magnified views of boxed areas in **b**. H&E (bright field views) and immunohistochemstry for type-I collagen (dark field views) were performed on serial sections. Green fluorescence indicates expression of type-I collagen. Asterisks, the remnants of calcium phosphate cement. (**d**) Quantification of bone regeneration. The ratio of the summation of the regenerated bone area to that of the original defect area (SRBA/SODA) in designated sections was histologically measured by NIH Image software. Data are means ± SD of five mice per group. *$P < 0.01$ versus GFP at 4 weeks after implantation. caALK6, constitutively active form of activin receptor-like kinase 6; DET, diethylenetriamine; PEG, poly(ethyleneglycol); Runx2, runt-related transcription factor 2.

In vivo gene delivery to the bone defect area on the mouse calvarial bone

The data so far have shown that a localized and sustained system to deliver polyplex nanomicelles was successfully developed *in vitro* using the calcium phosphate cement scaffold. To

investigate whether or not this system is effective for *in vivo* gene delivery, the scaffold was molded to the fitting shape and implanted in mouse calvarial bone defects. After implantation of the scaffold containing polyplex nanomicelles with GFP pDNA, successfully transfected recipient cells were observed across a few layers from the implant surface by immunohistochemical analyses (**Figure 7**). The intensity of the staining was strongest in cells immediately adjacent to the scaffold, gradually declining with distance.

To investigate the therapeutic potential of this system, polyplex nanomicelles containing pDNAs expressing a caALK6 and Runx2, by which the osteogenic differentiation was induced on the calvarial cells *in vitro* (**Figure 3**), were incorporated into the calcium phosphate cement scaffold and implanted in the same model. At 2 weeks after implantation, no bone formation occurred in either the control group transfected with the GFP-expressing pDNA or the treatment group transfected with caALK6 + Runx2 expressing pDNA (**Figure 8a**). At 4 weeks after implantation, however, substantial bone formation covering the entire lower surface of the implant was induced only in the treatment group (**Figure 8b**), as confirmed by the quantitative analysis of the regenerated bone area (**Figure 8d**). The regenerated bone tissues exhibited a lamellar structure containing osteocyte-like cells and strongly expressed the type-I collagen protein (**Figure 8c**). On the other hand, the incorporation of neither the LPEI nor the FuGENE6 complex into the calcium phosphate cement scaffold generated any apparent bone formation at 4 weeks (data not shown). It should be noted that no sign of inflammation was observed in any group (**Figure 8a–c**). The results so far indicate that the polyplex nanomicelles incorporated into the calcium phosphate cement scaffold transfected the foreign genes to the cells in the vicinity of the scaffold, leading to a considerable increase in the rate of bone formation via the induction of osteogenic differentiation.

DISCUSSION

Many clinical fields demand useful non-viral gene delivery systems that satisfy high standards of both efficacy of gene introduction and low toxicity.[37] Bone tissue engineering would be a promising field; however, only a few trials have been reported so far. Bright *et al.* used a naked pDNA expressing OP-1 (BMP-7) gene, which was incorporated into a collagen scaffold, for a rat model of lumbar interbody arthrodesis.[38] Although bone formation was stimulated after 4 weeks, it was not as extensive as that observed after the injection of recombinant human OP-1 protein, in spite of considerably high dose of pDNA (250 μg/rat). Huang *et al.* combined poly(lactic-co-glycolic acid) scaffolds with 200 μg of condensed pDNA encoding BMP4 using branched PEI and implanted the scaffolds into rat cranial defects.[39] They successfully induced bone regeneration at the defect edges; however, osteoid and mineralized tissue was significantly increased after 15 weeks of implantation. The disparity between our results and theirs presumably resulted from the difference in the osteogenic signals. However, some toxic effects of PEI should also be taken into consideration: PEI was reported to be an apoptotic agent,[40] and indeed in our results it showed appreciable cytotoxicity (**Figures 1b** and **2b**) and an inability to induce differentiation. Directly comparing the capacity of their versus our method was not possible because Huang *et al.* did not provide data on the actual transfection efficiency; however, some negative effects of PEI on the cells in the vicinity of the scaffold may have caused the delayed induction of bone regeneration.

The considerably low dose of pDNA (1.3 μg/mouse) is also characteristic in our system. In previous studies of *in vivo* bone formation by non-viral gene delivery systems, a larger amount of pDNA (100 μg to 1 mg) was used.[38,39,41] We assume that this may be attributed to the capacity of polyplex nanomicelles to stably retain pDNA even in the scaffolds. Moreover, using the combination of osteogenic genes *caALK6* and *Runx2* contributed to the efficient osteoconductivity of our system. The cooperative action of this combination occurred through protein stabilization of core binding factor beta (Cbfb) and through induction of Runx2–Cbfb complex formation and its DNA binding, leading to the efficient induction of osteogenic differentiation.[34]

FuGENE6 has often been reported to have excellent transfection efficiency *in vitro*, including the induction of cell differentiation.[29–33] Indeed, in our results shown in **Figure 3**, comparable induction of osteocalcin expression was observed by both FuGENE6 and polyplex nanomicelles on day 5. It is interesting to note that, although the gene expressions evaluated by luciferase were consistently higher in FuGENE6 until day 10 (**Figure 5**), the osteocalcin induction was more remarkable in the nanomicelles on day 10 (**Figure 3**). The marked difference in gene expression profiles between nanomicelles and FuGENE6—especially when evaluated by mRNA expression—might influence the outcome of cell differentiation, which requires complex intracellular processes over an extended period. It is also possible that some toxicologic effects of the reagents might influence the cell reactivity, since many lipid-based transfection reagents were reported to induce changes in the expression of endogenous genes.[42] The study of toxicologic or pharmacologic effects of bioactive materials that might alter responses to delivered drugs or genes is now attracting attention as polymer (material) genomics.[43] From this standpoint, we have started comprehensive analyses of cell bioactivities after various transfection procedures, including the study of endogenous gene expression profiles using complementary DNA arrays. These results will be reported elsewhere in the near future.

The polyplex nanomicelles composed of PEG-b-P[Asp-(DET)] block copolymer and pDNA have demonstrated promising features for bone-regenerative gene therapy. The characteristics are summarized as: (i) good transfection efficiency with minimal cytotoxicity; (ii) sustained gene expression profile, which may be beneficial to cell differentiation; and (iii) excellent *in vivo* availability. Worth noting is that the enhancement of bone regeneration in this study was achieved without cell transplantation. Although the use of cell sources such as stem cells has been widely investigated, there remain many concerns for clinical application, such as the difficulty of finding an ideal cell source that meets both quality and quantity demands while also satisfying the concerns of medical costs and health risks.[44,45] Thus, it is desirable that cell transplantation be supplemented or replaced by innovations in other components of tissue engineering, signals, and scaffolds.

In conclusion, we developed a new gene delivery system applicable to bone regenerative medicine. This polyplex nanomicelle showed high biocompatibility as well as a capacity for regulated gene transfer, inducing a remarkable increase in the bone regeneration rate in a bone defect model. This system holds much promise for constructing a practical gene-activated matrix for tissue engineering. Moreover, this technology will help realize therapeutic applications of gene therapy requiring safe and regulated gene expressions.

MATERIALS AND METHODS

Materials. pDNAs encoding luciferase (pGL3-control, 5,256bp) (Promega, Madison, WI) and GFP (pEGFP-C1, 4,700bp) (Clontech, Palo Alto, CA) were amplified in competent DH5α *Escherichia coli* and purified using EndoFree Plasmid Maxi or Mega Kits (Qiagen, Hilden, Germany). pCMV5 pDNA expressing hemagglutinin-tagged mouse caALK6 and pcDEF3 pDNA expressing Flag-tagged mouse Runx2 were generous gifts from M. Krüppel (Mt. Sinai Hospital, Toronto, Canada) and K. Miyazono (University of Tokyo, Tokyo, Japan), respectively. The DNA concentration was determined by reading the absorbance at 260nm. Commercially available transfection reagents, linear polyethylenimine (Exgen 500, M_w of LPEI = 22kd) and FuGENE6 were purchased from MBI Fermentas (Burlington, Canada) and Roche (Basel, Switzerland), respectively. Dulbecco's modified Eagle's medium and fetal bovine serum were purchased from Sigma-Aldrich (St. Louis, MO).

Synthesis and characterization of PEG-b-P[Asp-(DET)] block copolymer. The PEG-b-P[Asp-(DET)] block copolymer was synthesized as previously reported.[24] Briefly, PEG-poly(β-benzyl-L-aspartate) (PEG-PBLA) diblock copolymer was synthesized by the ring-opening polymerization of β-benzyl-L-aspartate *N*-carboxy-anhydride from the terminal primary amino group of α-methoxy-ω-amino PEG (M_w: 12,000; Nippon Oil and Fats, Tokyo, Japan). The copolymer thus prepared was confirmed to be unimodal with a narrow molecular weight distribution (M_w/M_n: 1.23) by gel-permeation chromatography, and the number of repeating units of BLA was calculated to be 68 by ^{1}H-NMR (data not shown). The N-terminal amino group of PEG-PBLA was then acetylated using acetic anhydride in dichloromethane solution to obtain PEG-PBLA-Ac. The obtained polymer was dissolved in distilled *N,N*-dimethylformamide (Wako Pure Chemical Industries, Osaka, Japan) and reacted with diethylenetriamine (DET) (Tokyo Kasei Kogyo, Tokyo, Japan) for 24 hours at 40°C under a dry argon atmosphere to undergo aminolysis of the benzyl side chain. After 24 hours, the solution was slowly dropped into 10% acetic acid solution and dialyzed (Spectra/por Membrane, molecular weight cut-off = 3,500, Rancho Dominquez, CA) against 0.01 N HCl and subsequently against distilled water. The final solution was lyophilized to obtain PEG-b-P[Asp-(DET)] as the hydrochloride salt form. ^{1}H-NMR confirmed the complete substitution of benzyl ester of the polymer with DET through the aminolysis reaction as well as the chemical structure of the obtained PEG-b-P[Asp-(DET)] block copolymer.

Preparation of pDNA carriers. The PEG-b-P[Asp-(DET)] block copolymer and pDNA were separately dissolved in 10mmol/l Tris–HCl buffer (pH 7.4). Both solutions were mixed at various nitrogen/phosphate (= (total amines in cationic segment)/(DNA phosphates)) and left overnight. The pDNA complexes with LPEI and FuGENE6 were prepared by mixing the pDNA solution and the reagents following the protocols provided by the manufacturers.

In vitro *transfection.* HEK293 cells were obtained from the Riken Cell Bank (Tsukuba, Japan). Mouse calvarial cells were isolated from calvariae of neonatal littermates. The experimental procedures were in accordance with the guidelines of the Animal Committee of the University of Tokyo. Calvariae were digested for 10 minutes at 37°C in an enzyme solution containing 0.1% collagenase and 0.2% dispase for five cycles. Cells isolated by the final four digestions were combined as an osteoblast population and cultured in Dulbecco's modified Eagle's medium containing 10% fetal bovine serum. Human synovial cells from rheumatoid arthritis patients were kindly provided by Dr. S. Tanaka (University of Tokyo).[46] Written informed consent for subsequent experiments was obtained from each patient.

For luciferase transfection assays, the cells were inoculated at a density of 2×10^4 cells/well in a 24-multiwell plate and cultured for 24 hours. After the culture medium was replaced with fresh medium containing 10% fetal bovine serum, pDNA carrier solution (33.3μg/ml, 22.5ml) was applied to each well. After several days of incubation, the cells were lysed and the luciferase gene expression was measured using a Luciferase Assay System (Promega, Madison, WI) and a Lumat LB9507 luminometer (Berthold, Bad Wildbad, Germany). The expression was normalized to protein concentrations of cell lysates. For the evaluation of sustained luciferase expression (**Figure 4**), the cells were seeded onto a 96-multiwell plate (6×10^3 cells/well). After incubation for 24 hours, 6μl of each pDNA carrier solution was added, followed by further incubation for up to day 10. The luminescence was measured by a GloMax 96 Microplate Luminometer (Promega, Madison, WI). For the GFP transfection assay, both the phase contrast and the fluorescence images were obtained by an Axiovert 100M microscope (Carl Zeiss, Oberkochen, Germany).

For the cytotoxicity assay, a 96-multiwell plate was used. After transfection as described above, the cells were incubated for 2 or 5 days and their viability was evaluated by an MTT assay (Cell Counting Kit-8, Dojindo, Kumamoto, Japan). Each well was measured by reading the absorbance at 450nm according to the protocol provided by the manufacturer. The results were expressed as the relative value (%) of the control cells, which were incubated in parallel without transfection.

Evaluation of mRNA expression. After transfection to mouse calvarial cells, the total RNA was collected using the RNeasy Mini Preparation Kit (Qiagen, Hilden, Germany) according to the manufacturer's protocol. Gene expression was analyzed by quantitative PCR. Using the Quantitect SYBR Green PCR Kit (Qiagen, Hilden, Germany), 20ng of total RNA was analyzed in a final volume of 20μl according to the manufacturer's protocol. Reverse transcription was performed for 30 minutes at 50°C followed by PCR: 40 thermal cycles of 15 seconds at 94°C, 30 seconds at 55°C, and 30 seconds at 72°C using an ABI Prism 7500 Sequence Detector (Applied Biosystems, Foster City, CA). Each mRNA expression was normalized to levels of mouse β-actin mRNA, also determined by quantitative reverse transcription-PCR, from the same total RNA samples. The following primers were used: osteocalcin, forward primer (AAGCAGGAGGGC AATAAGGT) and reverse primer (TTTGTAGGCGGTCTTCAAGC); mouse ALK6, forward primer (CACCAAGAAGGAGGATGGAG) and reverse primer (CTAGACATCCAGAGGTGACAACAG); mouse Runx2, forward primer (CCCAGCCACCTTTACCTACA) and reverse primer (TATGGAGTGCTGCTGGTCTG); luciferase, forward primer (TTGA CCGCCTGAAGTCTCTGA) and reverse primer (ACACCTGCGTCGA AGATGTTG); mouse β-actin, forward primer (AGATGTGGATCAG CAAGCAG) and reverse primer (GCGCAAGTTAGGTTTTGTCA). As for luciferase, the gene expression presented as the light units was also evaluated in parallel.

In vitro *transfection from gene-containing scaffolds.* To prepare the scaffolds containing gene carriers, the PEG-P[Asp-(DET)]/pDNA micelles were mixed with calcium phosphate paste (BIOPEX-R; Mitsubishi Pharma, Osaka, Japan). According to the manufacturer's information, the powder consists of particles (2–5mm in diameter) of α-tricalcium phosphate (75% wt), tetracalcium phosphate monoxide (18% wt), dicalcium phosphate dibasic (5% wt), and hydroxyapatite (2% wt); the aqueous solution contains sodium chondroitin sulfate (5.4%) and sodium succinate

(13%). For solidification, 1.0 g of the powder was manually mixed (at low shear rates) with 233 μl of the solution containing pDNAs. After solidification, the cement containing 1.3 μg of pDNA was placed onto the upper chamber of a BD Falcon Cell Culture Insert for 12-well plates (1.0 μm pore size, Becton Dickinson, Franklin Lakes, NJ), and HEK293 cells were plated onto the lower chamber. Five days later, luciferase assay was performed as described. The level of luciferase expression was normalized to the protein concentrations of cell lysates.

In vivo *gene delivery for the bone defect area on the mouse skull bone.* In this study, the 4 mm defects in diameter were chosen as the mouse bone defect model.[47,48] We have observed that the mouse calvarial defects (4 mm in diameter) could not be covered spontaneously with regenerated bone within 8 weeks after operation, although significant bone formation was observed at the defect edge (data not shown). Thus, the bone regeneration was evaluated within or at 4 weeks after gene delivery.

For the generation of bone defects, mice were anesthetized with ketamine/xylazine (80 mg/kg and 5 mg/kg) solution through intraperitoneal injection, and a linear incision was made along the sagittal suture from the frontal bone to the center of the occipital bone. A round craniotomy defect (4 mm in diameter) was manually created on both parietal bones with a sterile disposable trephine (Kai Industries, Gifu, Japan).[47] Calcium phosphate paste was used to fill in the defects, and then the incisions were sutured. The mice were killed at 2, 4, or 8 weeks after the operation for radiologic, histologic, or immunohistologic analyses, respectively. Animal experiments were performed according to the protocol approved by the Animal Care and Use Committee of the University of Tokyo.

Assessment of bone regeneration. After the mice were asphyxiated with carbon dioxide, the calvarias were removed. Tissue preparation, hematoxylin and eosin staining, and immunohistologic analysis using a rabbit polyclonal antibody against GFP (Molecular Probes, Eugene, OR) or a rabbit polyclonal antibody against type-I collagen (LSL, Tokyo, Japan) were performed as described.[49] To evaluate the extent of bone regeneration, serial coronal sections of the implantation site were performed at 0.5, 1, 1.5, 2, 2.5, 3, and 3.5 mm from the rostral end and then stained with hematoxylin and eosin. For each section, the original defect area and the regenerated bone area were measured by NIH Image software. The ratio of the summation of the regenerated bone area to that of the original defect area (SRBA/SODA) was calculated and used as the index of bone regeneration.

ACKNOWLEDGMENTS

We thank Michael Klüppel (Mount Sinai Hospital) and Kohei Miyazono (University of Tokyo) for pDNAs expressing caALK6 and Runx2, respectively. We also appreciate Sakae Tanaka (University of Tokyo) for providing human synovial cells. This work was supported by Grants-in-Aid for Scientific Research from the Japanese Ministry of Education, Culture, Sports, Science and Technology (#15390452 and #17390530), Health Science Research Grants from the Japanese Ministry of Health, Labor and Welfare (#H16-regenerative medicine-008), and the Core Research Program for Evolutional Science and Technology (CREST) from the Japan Science and Technology Corporation (JST).

SUPPLEMENTARY MATERIAL

Figure S1. Zeta-potential of polyplex nanomicelles and pDNA complexes with P[Asp-(DET)], the cationic segment of the block copolymer used in this study.

Figure S2. GFP gene expression in human synovial cells.

Figure S3. GFP gene expression in mouse calvarial cells.

Figure S4. *In vitro* transfection by polyplex nanomicelles incorporated into calcium phosphate cement scaffold.

REFERENCES

1. Bucholz, RW, Heckman, JD (2006). *Rockwood and Green's Fractures in Adults*. Lippincott Williams & Wilkins: Philadelphia, PA. 587pp.
2. Banwart, JC, Asher, MA and Hassanein, RS (1995). Iliac crest bone graft harvest donor site morbidity. A statistical evaluation. *Spine* **20**: 1055–1060.
3. Arrington, ED, Smith, WJ, Chambers, HG, Bucknell, AL and Davino, NA (1996). Complications of iliac crest bone graft harvesting. *Clin Orthop Relat Res* **329**: 300–309.
4. Langer, R and Vacanti, JP (1993). Tissue engineering. *Science* **260**: 920–926.
5. Bruder, SP and Caplan, AI (2000). *Principles of Tissue Engineering*. Academic Press: San Diego, CA. 683pp.
6. Winn, SR, Hu, Y, Sfeir, C and Hollinger, JO (2000). Gene therapy approaches for modulating bone regeneration. *Adv Drug Deliv Rev* **42**: 121–138.
7. Baltzer, AW and Lieberman, JR (2004). Regional gene therapy to enhance bone repair. *Gene Ther* **11**: 344–350.
8. Katagiri, T and Takahashi, N (2002). Regulatory mechanisms of osteoblast and osteoclast differentiation. *Oral Dis* **8**: 147–159.
9. Long, F, Chung, UI, Ohba, S, McMahon, J, Kronenberg, HM and McMahon, AP (2004). Ihh signaling is directly required for the osteoblast lineage in the endochondral skeleton. *Development* **131**: 1309–1318.
10. Komori, T (2003). Requisite roles of Runx2 and Cbfb in skeletal development. *J Bone Miner Metab* **21**: 193–197.
11. Patel, MS and Karsenty, G (2002). Regulation of bone formation and vision by LRP5. *N Engl J Med* **346**: 1572–1574.
12. Ogata, N, Chikazu, D, Kubota, N, Terauchi, Y, Tobe, K, Azuma, Y *et al.* (2000). Insulin receptor substrate-1 in osteoblast is indispensable for maintaining bone turnover. *J Clin Invest* **105**: 935–943.
13. Govender, S, Csimma, C, Genant, HK, Valentin-Opran, A, Amit, Y, Arbel, R *et al.* (2002). Recombinant human bone morphogenetic protein-2 for treatment of open tibial fractures: a prospective, controlled, randomized study of four hundred and fifty patients. *J Bone Joint Surg Am* **84-A**: 2123–2134.
14. Valentin-Opran, A, Wozney, J, Csimma, C, Lilly, L and Riedel, GE (2002). Clinical evaluation of recombinant human bone morphogenetic protein-2. *Clin Orthop Relat Res* **395**: 110–120.
15. Gerstenfeld, LC, Cullinane, DM, Barnes, GL, Graves, DT and Einhorn, TA (2003). Fracture healing as a post-natal developmental process: molecular, spatial, and temporal aspects of its regulation. *J Cell Biochem* **88**: 873–884.
16. Howell, TH, Fiorellini, J, Jones, A, Alder, M, Nummikoski, P, Lazaro, M *et al.* (1997). A feasibility study evaluating rhBMP-2/absorbable collagen sponge device for local alveolar ridge preservation or augmentation. *Int J Periodontics Restorative Dent* **17**: 124–139.
17. Zhao, M, Zhao, Z, Koh, JT, Jin, T and Franceschi, RT (2005). Combinatorial gene therapy for bone regeneration: cooperative interactions between adenovirus vectors expressing bone morphogenetic proteins 2, 4, and 7. *J Cell Biochem* **95**: 1–16.
18. Riew, KD, Wright, NM, Cheng, S, Avioli, LV and Lou, J (1998). Induction of bone formation using a recombinant adenoviral vector carrying the human BMP-2 gene in a rabbit spinal fusion model. *Calcif Tissue Int* **63**: 357–360.
19. Rutherford, RB, Moalli, M, Franceschi, RT, Wang, D, Gu, K and Krebsbach, PH (2002). Bone morphogenetic protein-transduced human fibroblasts convert to osteoblasts and form bone *in vivo*. *Tissue Eng* **8**: 441–452.
20. Schek, RM, Hollister, SJ and Krebsbach, PH (2004). Delivery and protection of adenoviruses using biocompatible hydrogels for localized gene therapy. *Mol Ther* **9**, 130–138.
21. Gafni, Y, Pelled, G, Zilberman, Y, Turgeman, G, Apparailly, F, Yotvat, H *et al.* (2004). Gene therapy platform for bone regeneration using an exogenously regulated, AAV-2-based gene expression system. *Mol Ther* **9**: 587–595.
22. Lundstrom, K (2003). Latest development in viral vectors for gene therapy. *Trends Biotechnol* **21**: 117–122.
23. Egermann, M, Lill, CA, Griesbeck, K, Evans, CH, Robbins, PD, Schneider, E *et al.* (2006). Effect of BMP-2 gene transfer on bone healing in sheep. *Gene Ther* **13**: 1290–1299.
24. Kanayama, N, Fukushima, S, Nishiyama, N, Itaka, K, Jang, WD, Miyata, K *et al.* (2006). A PEG-based biocompatible block catiomer with high buffering capacity for the construction of polyplex micelles showing efficient gene transfer toward primary cells. *ChemMedChem* **1**: 439–444.
25. Harada-Shiba, M, Yamauchi, K, Harada, A, Takamisawa, I, Shimokado, K and Kataoka, K (2002). Polyion complex micelles as vectors in gene therapy—pharmacokinetics and *in vivo* gene transfer. *Gene Ther* **9**: 407–414.
26. Itaka, K, Harada, A, Nakamura, K, Kawaguchi, H and Kataoka, K (2002). Evaluation by fluorescence resonance energy transfer of the stability of nonviral gene delivery vectors under physiological conditions. *Biomacromolecules* **3**: 841–845.
27. Itaka, K, Yamauchi, K, Harada, A, Nakamura, K, Kawaguchi, H and Kataoka, K (2003). Polyion complex micelles from plasmid DNA and poly(ethylene glycol)-poly(L-lysine) block copolymer as serum-tolerable polyplex system: physicochemical properties of micelles relevant to gene transfection efficiency. *Biomaterials* **24**: 4495–4506.
28. Boussif, O, Lezoualc'h, F, Zanta, MA, Mergny, MD, Scherman, D, Demeneix, B *et al.* (1995). A versatile vector for gene and oligonucleotide transfer into cells in culture and *in vivo*: polyethylenimine. *Proc Natl Acad Sci USA* **92**: 7297–7301.
29. Hellgren, I, Drvota, V, Pieper, R, Enoksson, S, Blomberg, P, Islam, KB *et al.* (2000). Highly efficient cell-mediated gene transfer using non-viral vectors and FuGene6: *in vitro* and *in vivo* studies. *Cell Mol Life Sci* **57**: 1326–1333.
30. Weiskirchen, R, Kneifel, J, Weiskirchen, S, van de Leur, E, Kunz, D and Gressner, AM (2000). Comparative evaluation of gene delivery devices in primary cultures of rat hepatic stellate cells and rat myofibroblasts. *BMC Cell Biol* **1**: 4.
31. Lee, MJ, Cho, SS, You, JR, Lee, Y, Kang, BD, Choi, JS *et al.* (2002). Intraperitoneal gene delivery mediated by a novel cationic liposome in a peritoneal disseminated ovarian cancer model. *Gene Ther* **9**: 859–866.
32. Elmadbouh, I, Rossignol, P, Meilhac, O, Vranckx, R, Pichon, C, Pouzet, B *et al.* (2004). Optimization of *in vitro* vascular cell transfection with non-viral vectors for *in vivo* applications. *J Gene Med* **6**: 1112–1124.
33. Tinsley, RB, Faijerson, J and Eriksson, PS (2006). Efficient non-viral transfection of adult neural stem/progenitor cells, without affecting viability, proliferation or differentiation. *J Gene Med* **8**: 72–81.
34. Ohba, S, Ikeda, T, Kugimiya, F, Yano, F, Lichtler, AC, Nakamura, K *et al.* (2007). Identification of a potent combination of osteogenic genes for bone

regeneration using embryonic stem (ES) cell-based sensor. *FASEB J* (epub ahead of print).
35. Hunter, AC (2006). Molecular hurdles in polyfectin design and mechanistic background to polycation induced cytotoxicity. *Adv Drug Deliv Rev* **58**: 1523–1531.
36. Bonadio, J, Smiley, E, Patil, P and Goldstein, S (1999). Localized, direct plasmid gene delivery *in vivo*: prolonged therapy results in reproducible tissue regeneration. *Nat Med* **5**: 753–759.
37. Verma, IM and Somia, N (1997). Gene therapy—promises, problems and prospects. *Nature* **389**: 239–242.
38. Bright, C, Park, YS, Sieber, AN, Kostuik, JP and Leong, KW (2006). *In vivo* evaluation of plasmid DNA encoding OP-1 protein for spine fusion. *Spine* **31**: 2163–2172.
39. Huang, YC, Simmons, C, Kaigler, D, Rice, KG and Mooney, DJ (2005). Bone regeneration in a rat cranial defect with delivery of PEI-condensed plasmid DNA encoding for bone morphogenetic protein-4 (BMP-4). *Gene Ther* **12**: 418–426.
40. Moghimi, SM, Symonds, P, Murray, JC, Hunter, AC, Debska, G and Szewczyk, A (2005). A two-stage poly(ethylenimine)-mediated cytotoxicity: implications for gene transfer/therapy. *Mol Ther* **11**: 990–995.
41. Geiger, F, Bertram, H, Berger, I, Lorenz, H, Wall, O, Eckhardt, C *et al.* (2005). Vascular endothelial growth factor gene-activated matrix (VEGF165-GAM) enhances osteogenesis and angiogenesis in large segmental bone defects. *J Bone Miner Res* **20**: 2028–2035.
42. Omidi, Y, Hollins, AJ, Benboubetra, M, Drayton, R, Benter, IF and Akhtar, S (2003). Toxicogenomics of non-viral vectors for gene therapy: a microarray study of lipofectin- and oligofectamine-induced gene expression changes in human epithelial cells. *J Drug Target* **11**: 311–323.
43. Kabanov, AV, Batrakova, EV, Sriadibhatla, S, Yang, Z, Kelly, DL and Alakov, VY (2005). Polymer genomics: shifting the gene and drug delivery paradigms. *J Control Release* **101**: 259–271.
44 Buttery, LD, Bourne, S, Xynos, JD, Wood, H, Hughes, FJ, Hughes, SP *et al.* (2001). Differentiation of osteoblasts and *in vitro* bone formation from murine embryonic stem cells. *Tissue Eng* **7**: 89–99.
45. Jiang, Y, Vaessen, B, Lenvik, T, Blackstad, M, Reyes, M and Verfaillie, CM (2002). Multipotent progenitor cells can be isolated from postnatal murine bone marrow, muscle, and brain. *Exp Hematol* **30**: 896–904.
46. Seto, H, Kamekura, S, Miura, T, Yamamoto, A, Chikuda, H, Ogata, T *et al.* (2004). Distinct roles of Smad pathways and p38 pathways in cartilage-specific gene expression in synovial fibroblasts. *J Clin Invest* **113**: 718–726.
47. Hirata, K, Tsukazaki, T, Kadowaki, A, Furukawa, K, Shibata, Y, Moriishi, T *et al.* (2003). Transplantation of skin fibroblasts expressing BMP-2 promotes bone repair more effectively than those expressing Runx2. *Bone* **32**: 502–512.
48. Cowan, CM, Shi, YY, Aalami, OO, Chou, YF, Mari, C, Thomas, R *et al.* (2004). Adipose-derived adult stromal cells heal critical-size mouse calvarial defects. *Nat Biotechnol* **22**: 560–567.
49. Kugimiya, F, Kawaguchi, H, Kamekura, S, Chikuda, H, Ohba, S, Yano, F *et al.* (2005). Involvement of endogenous bone morphogenetic protein (BMP) 2 and BMP6 in bone formation. *J Biol Chem* **280**: 35704–35712.

In Vivo Antitumor Activity of the Folate-Conjugated pH-Sensitive Polymeric Micelle Selectively Releasing Adriamycin in the Intracellular Acidic Compartments

Younsoo Bae,[†,‡] Nobuhiro Nishiyama,[†,‡] and Kazunori Kataoka*[,†,‡,§]

Center for Disease Biology and Integrative Medicine, Graduate School of Medicine, The University of Tokyo, 7-3-1 Hongo, Bunkyo-ku, Tokyo 113-0033, Japan, and Center for NanoBio Integration and Department of Materials Engineering, The University of Tokyo, 7-3-1 Hongo, Bunkyo-ku, Tokyo 113-8656, Japan. Received December 26, 2006; Revised Manuscript Received March 2, 2007

Cancer treatment efficacy and safety of the environmentally sensitive polymeric micelle drug carriers were significantly increased by optimizing the number of ligands on their surface. These micelles were designed to target the cancerous tumors through the interaction between folate and its receptors that overexpress on the cancer cell membrane while achieving pH-controlled drug release in the intracellular acidic compartments such as endosomes and lysosomes. In order to elucidate the effects of folate on cytotoxicity, biodistribution, anticancer activity, and pharmacological properties, folate concentration on the surface of the micelles was controlled by precise synthesis of two different amphiphilic block copolymers that self-assemble into spherical micelles, folate–poly(ethylene glycol)–poly(aspartate-hydrazone-adriamycin) with γ-carboxylic acid activated folate and methoxy-poly(ethylene glycol)–poly(aspartate-hydrazone-adriamycin) without folate. It is of significance that, although folate conjugation induced an extremely small change in tumor accumulation of the micelles, folate-conjugated micelles showed lower in vivo toxicity and higher antitumor activity over a broad range of the dosage from 7.50 to 26.21 mg/kg, which was 5-fold broader than free drugs.

INTRODUCTION

Precise control of the amount and uniform distribution of ligands on nanoparticles is one of the most challenging assignments in the design of polymeric drug carriers for successful active drug targeting (*1*–*3*). Indeed, a large number of studies have shown that active drug targeting is promising for effective cancer treatment (*4*–*7*). However, the questions about how many ligands are necessary for achieving efficient active drug targeting of the polymeric drug carriers are still controversial and remain to be elucidated further. In particular, when such drug carriers are tailored to deliver anticancer drugs to cancer cells systemically, it is of significant importance to confirm whether the ligand conjugation maintains their pharmacokinetic properties without decreasing antitumor activity. It is because anticancer drugs are normally highly toxic, inducing serious side effects, and although ligands can increase the interaction between the drug carriers and targeted cells in the body, they might also induce an increase in the cellular interaction with nontargeted cells, that we are not willing to deliver drugs. In order to answer these questions, we have to prepare first a drug carrier with optimal amounts of ligands, whose chemical and biological properties are fairly well established and then ascertain whether ligand installation induces any change in its biological properties.

The rationales for tumor-specific drug delivery with polymers have been reported during the past decades and are based on the characteristics of tumor tissues such as disordered and leaky vasculatures, a thick extracellular matrix, and other microenvironmental peculiarities including the hypoxic environment, expression of cancer-specific receptors, and excessive secretion of cytokines (*8*–*9*). One of the widely accepted methodologies for polymeric drug delivery is to target leaky tumor vessels and the poorly developed lymphatic drainage in the tumor tissues so that polymers and their drug conjugates can pass the tumor blood vessel wall and then accumulate in tumor tissue for a prolonged time. This methodology is explained as the enhanced permeability and retention (EPR) effect, providing the most probable theory for passive drug targeting (*10*). Nevertheless, recent studies have revealed that tumor-targeting drug delivery cannot be completely achieved only by the EPR effect because polymeric drug carriers often encounter difficulties in accessing cancer cells in the deeper place of the tumor tissues or in interacting with the targeted cells after accumulation (*11*, *12*). Polymeric drug carriers are normally required to have biocompatibility and high molecular weight to prevent protein adsorption that induces recognition by the body defense system and to increase the tumor accumulation via the EPR effect, respectively. However, these efforts frequently result in low cellular uptake of polymeric drug carriers after extravasation, reducing the actual drug concentration within the tumor due to the stagnation around the tumor tissue. As a result, we should inject polymeric drug carriers with a higher amount compared to free drugs to deliver a sufficient amount of drugs to the tumor. This is also the reason the current polymeric drug delivery systems urgently need to improve their targeting efficiency. From these aspects, active targeting has been believed to clear the problems by facilitating polymeric drug delivery systems (*13*). Active targeting can be achieved by installing ligands to the polymers or polymer assemblies so that they can interact with receptors that express on the targeted sites such as cancer cell membranes. Nevertheless, it is obvious that active targeting

* To whom correspondence should be addressed: Kazunori Kataoka, Ph.D. Professor, Department of Materials Engineering, Graduate School of Engineering, The University of Tokyo, 7-3-1 Hongo, Bunkyo-ku, Tokyo 113-8656, Japan. Phone +81-3-5841-7138, Fax +81-3-5841-7139, E-mail: kataoka@bmw.t.u-tokyo.ac.jp.

† Graduate School of Medicine.

‡ Center for NanoBio Integration.

§ Department of Materials Engineering.

10.1021/bc060401p CCC: $37.00
Published on Web 05/09/2007

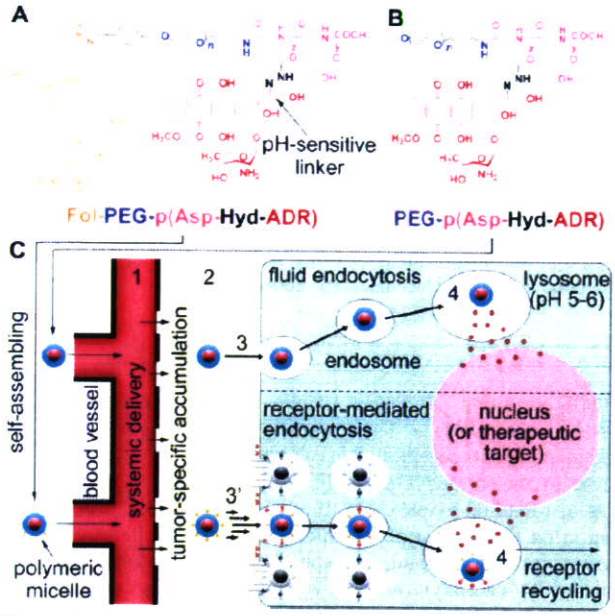

Figure 1. Design of polymeric micelles and the rationale for active drug delivery. Chemical structures of folate−poly(ethylene glycol)−poly(aspartate-hydrazone-adriamycin) and methoxy-poly(ethylene glycol)−poly(aspartate-hydrazone-adriamycin) block copolymers (A and B). As shown in panel C, these polymers can self-assemble into the polymeric micelles that can effectively achieve systemic drug delivery and tumor-specific accumulation (1 and 2). The micelles are then uptaken by the cancer cells via fluid endocytosis (3) or receptor-mediated endocytosis (3′) depending on surface design for accelerating endocytosis (e.g., folate conjugation). Anticancer drugs, adriamycin (ADR), that are conjugated through a pH-sensitive hydrazone bond can be released from the micelles in the acidic intracellular compartments such as endosomes or lysosomes where pH ranges from 5 to 6 (4).

cannot be achieved until passive targeting of drug carriers is successfully accomplished.

Amphiphilic block copolymers are useful tools for the preparation of supramolecular assemblies. By precisely controlling their molecular weight and the hydrophilic/hydrophobic balance, we can prepare spherical supramolecular nanoassemblies, also known as "the polymeric micelles", with a hydrophilic shell that envelopes a hydrophobic core (*14*). The polymeric micelle is considered to be one of the most successful polymeric drug carrier formulations, because it is characterized by high drug loading contents, prolonged blood circulation, and selective tumor accumulation (*15*). Most notably, their chemical, biological, and pharmacological properties have been widely studied, and thus we can easily investigate the effect of active targeting (*16, 17*). In this study, poly(ethylene glycol)−poly(β-benzyl-L-aspartate) block copolymers (PEG−PBLA) were synthesized for the basic platform for the preparation of the polymeric micelles, and these micelles were further functionalized to conjugate anticancer drugs and ligands. Figure 1 shows the chemical structures of the block copolymers used in this study. Anticancer drugs, adriamycin (ADR), were conjugated to the side chains of the core-forming poly(aspartic acid) block through a hydrazone linkage, which can be selectively cleaved under the acidic conditions with pH ranging from 5 to 6, corresponding to the intracellular vesicles such as the endosomes and lysosomes (*18*). In our previous studies, we have reported that this intracellular pH-sensitive polymeric micelle showed remarkably low toxicity and high in vivo efficacy (*19*). It was also confirmed that the pH-sensitive micelles can release drugs selectively by responding to a decrease in intracellular pH of the cell, and therefore, drug leakage from the micelles decreases during the blood circulation and tumor-specific drug delivery efficiency increases. In the meantime, folate was conjugated at the end of the shell-forming poly(ethylene glycol) (PEG) block for active targeting. Folate, an anionic form of folic acid, is a vitamin B9 that helps the production and maintenance of new cells. Originally, folate was necessary for the restoration of the DNA damage that may induce cancer. However, interestingly, cancer cells overexpress folate-binding proteins (FBPs) on their cell membranes (*20, 21*). This is probably due to the DNA replication that is supported by folate, which is also a prerequisite for the cancer growth. More interestingly, cancer cells are believed to reduce chemotherapeutical response by regulating intracellular folate concentration (*22*). Therefore, we can actively guide polymeric drug carriers to cancer cells in the body by folate conjugation (*23*). It must be noticed that FBP binding activity of folate drastically changes depending on its activated state, which is distinguished by an inactive α- and active γ-carboxyl activated form (*24*). Herein, we conjugated folate to PEG at its γ-carboxyl position to maintain its activity by precision synthesis as reported elsewhere (*25*−*27*).

The objectives of this research are to ascertain whether folate conjugation can enhance antitumor efficacy of the pH-sensitive micelles without deteriorating the characteristics of the micelles as a long-circulating drug carrier with high tumor accumulation, and to determine how much folate concentration is optimum for achieving effective passive and active drug targeting simultaneously. Such information would be beneficial to the future design and preparation of ligand-installed multifunctional polymeric drug carriers for cancer treatment.

EXPERIMENTAL PROCEDURES

Materials and Devices. Acetic anhydride (AA), chloroform ($CHCl_3$), *N,N*-dimethyl formamide (DMF), dimethyl sulfoxide (DMSO), hexane, methanol (MeOH), methanesulfonyl chloride (CH_3SO_2Cl), triethylamine (TEA), trifluoroacetic acid (TFA), trifluoroacetic anhydride (TFAA), and tetrahydrofuran (THF) were purchased from Wako Pure Chemical Industries, Japan. DMF, hexane, and THF were distilled twice following standard procedures. Carbazic acid *tert*-butyl ester (CAt-BE) and potassium carbonate (K_2CO_3) were purchased from Tokyo Kasei Organic Chemicals, Japan. These chemicals were used without further purification. Daunorubicin (DAU), folic acid (Fol), 4-(diethoxymethyl)benzaldehyde, and sodium borohydride ($NaBH_4$) were purchased from Sigma Chemical, U.S.A. Ethylene oxide (EO) was from Sumitomo Seika Chemicals, Japan, and dried over calcium hydride followed by distillation. β-Benzyl-L-aspartate (BLA) was from Sigma, and α-methoxy-ω-amino-poly(ethylene glycol) (MeO-PEG-NH_2) was from Nippon Oil and Fats, Japan. PEG was purified using an ion-exchange gel column (CM-Sephadex C-50, Amersham Pharmacia Biotech, U.S.A.) prior to the synthesis of the block copolymers. Adriamycin hydrochloride (ADR) was kindly provided by Nippon Kayaku, Japan, and its purity was checked by reversed-phase liquid chromatograpy (RPLC). Sephadex LH-20 gel was from Amersham Pharmacia Biotech, Sweden. Gel permeation chromatography (GPC) analysis was carried out using a TOSOH HLC-8220 equipped with TSK-GEL columns (G4000PWXL and G3000PWXL). Internal refractive index (RI) and ultraviolet−visible absorption (UV) detectors were used. DMF containing 10 mM of LiCl was used as an eluant at a flow rate of 0.8 mL/min at 40 °C. ^1H NMR spectra were measured with a JEOL EX300 spectrometer (JEOL, Japan). Flow cytometric analysis was performed with EPICS XL Flow Cytometry Systems (Beckman Coulter, U.S.A.). The multimode reader Mithras LB 940 (Berthold Technologies, U.S.A.) was used for in vitro cytotoxicity evaluation using a CellTiter-Glo luminescent cell viability assay kit (Promega, U.S.A.).

Cell Lines and Animals. A human pharyngeal cancer cell line KB was purchased from Health Science Research Resources Bank, Japan. Cells were cultured in Dulbecco's Modified Eagle cell culture Medium (DMEM, Sigma, U.S.A.) containing 10% FBS under a humidified atmosphere with 5% CO_2 at 37 °C. CD-1 nude mice (female, 6-week-old) were purchased from Charles River, Japan. The animals were cared for and all experiments were performed in compliance with the Guide for the Care and Use of Laboratory Animals as adopted and promulgated by the National Institutes of Health. The number of independent experiments is stated as n, and the experimental data are expressed as mean and mean ± SEM for relative and absolute values, respectively.

Synthesis of Self-Assembling Amphiphilic Block Copolymers. In this study, we synthesized two different types of self-assembling amphiphilic block copolymers for the preparation of the micelles, folate−poly(ethylene glycol)−poly(aspartate-hydrazone-adriamycin) [Fol−PEG−p(Asp-Hyd-ADR)] and methoxy-poly(ethylene glycol)−poly(aspartate-hydrazone-adriamycin) [PEG−p(Asp-Hyd-ADR)]. Synthesis methods for these block copolymers were previously reported elsewhere (*25*). Briefly, Fol−PEG−p(Asp-Hyd-ADR) was synthesized via seven steps as follows.

a. Synthesis of Heterobifunctional α-4-(Diethoxymethyl)-benzylacetal-ω-amine-poly(ethylene glycol) (aceBz-PEG-NH_2). 4-(Diethoxymethyl)benzaldehyde (5 g) was reduced with $NaBH_4$ (1 g) in dry ethanol (100 mL). Obtained 4-(diethoxymethyl)-benzylalcohol (0.19 g) was then mixed with potassium naphthalene (115 mg) in dry THF (30 mL) to prepare potassium 4-(diethoxymethyl)benzylalkoxide, followed by the addition of distilled EO (11.9 g) for anionic polymerization to obtain aceBz-PEG-OH. After 2 days of reaction at 25 °C, CH_3SO_2Cl (0.62 g) and TEA (0.82 g) were added to aceBz-PEG-OH in 25 mL of THF to prepare an intermediate product aceBz-PEG-OSO_2CH_3, which was then mixed with ammonia solution (25%) to produce aceBz-PEG-NH_2.

b. Selective Functionalization of Folic Acid at its γ-Position of the Glutamate Residue with Hydrazide (Fol-hyd). An excess amount of TFAA (3 mL) was added dropwisely to folic acid (2 g) in THF (20 mL) to prepare N_{10}-(trifluoroacetyl)pyrofolic acid. This pyrofolic acid (500 mg) was reacted with CAt-BE (1.6 g) in 20 mL of dry DMF at 40 °C overnight. Prepared folate-hydrazide-BOC was treated with TFA to obtain Fol−Hyd.

c. Preparation of β-benzyl-L-aspartate N-Carboxy Anhydride (BLA−NCA). 5.77 g of triphosgene was added to 10 g of β-benzyl-L-aspartate in 150 mL of dry THF at 40 °C, and the reaction was allowed to proceed until the solution became clear. Prepared β-benzyl-L-aspartate *N*-carboxy anhydride (BLA−NCA) was purified by recrystallization from hexane.

d. Ring-Opening Polymerization of BLA−NCA by Using aceBz-PEG-NH_2 as a Macroinitiator to Obtain 4-(Diethoxymethyl)benzyl Acetal−poly(ethylene glycol)−poly(β-benzyl-L-aspartate) (aceBz−PEG−PBLA). 6 g of aceBz−PEG−NH_2 with molecular weight of 12 000 and 5 g of BLA−NCA were dissolved in 30 mL and 10 mL of DMSO, respectively. NCA solution was added to PEG solution at 40 °C, and the reaction was allowed to proceed for 2 days.

e. ω-Amino Group Protection for aceBz−PEG−PBLA Block Copolymers, Followed by α-Acetal Group Deprotection and Subsequent Conjugation of Fol−hyd at the End of the PEG Chain (Fol−PEG−PBLA). The ω-amino group of aceBz−PEG−PBLA was protected by AA to prevent dimerization between aldehyde−benzyl−poly(ethylene glycol)−poly(β-benzyl-L-aspartate) (CHO−Bz−PEG−PBLA) block copolymers, which can be prepared by deprotecting acetal groups of aceBz−PEG−PBLA with 0.1 N HCl aqueous solution. End-group protected CHO−Bz−PEG−PBLA (250 mg) was then mixed with Fol−Hyd (50 mg) in dry DMF to prepare Fol−PEG−PBLA.

f. Substitution Benzyl Esters at the Side Chain of Fol−PEG−PBLA with Drug-Binding Hydrazide Groups to Prepare Fol−PEG−p(Asp-Hyd). 500 mg of Fol−PEG−PBLA was dissolved in 10 mL of dry DMF, and anhydrous hydrazine (0.62 mg) was added to the solution. The reaction was allowed to proceed at 40 °C for 2 h, followed by deprotection of remained benzyl groups with 0.1 N NaOH aqueous solution at 25 °C. Polymers were dialyzed against 0.25% ammonia solution and collected by freeze-drying.

g. Conjugation of ADR at Its 13-C Carbonyl with the Hydrazide Groups of Fol−PEG−p(Asp-Hyd) through a pH-Sensitive Schiff Base Linkage. Fol−PEG−p(Asp-Hyd) (100 mg) in 50 mL of DMSO was mixed with an excess amount of ADR-HCl (100 mg) with respect to drug-binding hydrazide residues. The mixed solution was stirred at room temperature for 3 days. After precipitation from ether, Fol−PEG−p(Asp-Hyd-ADR) was redissolved in 10 mL of DMF and purified by gel filtration using a Sephadex LH-20 column. In the case of PEG−p(Asp-Hyd-ADR), MeO-PEG-NH_2 was used as a macroinitiator for BLA−NCA polymerization at step (d) instead of aceBz−PEG-NH_2, following the procedures from steps (e) to (g).

Preparation of the Folate-Conjugated pH-Sensitive Polymeric Micelles. The folate-conjugated pH-sensitive polymeric micelles were prepared from Fol−PEG−p(Asp-Hyd-ADR) alone or in combination with PEG−p(Asp-Hyd-ADR) block copolymers in various molar ratios to change folate contents (0%, 1%, 2%, 5%, 10%, 25%, 50%, and 100%). We distinguish the micelles from Fol−PEG-p(Asp-Hyd-ADR) and PEG−p(Asp-Hyd-ADR) by the notations of FMA and MA, which denote folate-conjugated micellar adriamycin and micellar adriamycin, respectively. For the preparation of FMA and MA, 250 mg of each Fol−PEG−p(Asp-Hyd-ADR) and PEG−p(Asp-Hyd-ADR) were dissolved in 5 mL of DMSO. Polymer solutions were then added dropwise into 95 mL of Tris−HCl buffer solution (10 mM, pH 7.4), sonicated at 25 °C for 10 min, and diluted further with 900 mL of Tris−HCl buffer. The polymer solutions were concentrated by Amicon Ultra-15 Centrifugal Filter Units (Millipore, U.S.A.) with molecular weight cutoff (MWCO) 30 000 kDa. 12 mL of the solutions in each swinging bucket rotor were spun at 1500 *g* at 25 °C for 15 min. During repetitive centrifugation, additional Tris−HCl buffer was added to the solutions until DMSO was completely removed. Concentrated micelle solutions were filter-sterilized and stored in aliquots at 4 °C for future use. Drug concentration was determined by UV at 490 nm, based on the calibration curve of free ADR.

Table 1. Polymer Compositions

compound	composition[a]	polydispersity index[d] (Mw/Mn)	drug loading content (wt %)
PEG-PBLA	12−42[b]	1.12	
Fol-PEG-PBLA	12−40[b]	1.14	
PEG-p(Asp-Hyd-ADR)	12−42−33−15[c]		33.84
Fol-PEG-p(Asp-Hyd-ADR)	12−40−34−14[c]		34.32

[a] The compositions of the block copolymers are abbreviated *X*−*Y* and *X*−*Y*−*Z*−*A*. The letter *X* stands for molecular weight × 10^{-3} of poly(ethylene glycol), while *Y*, *Z*, and *A* denote the numbers of aspartic acid, hydrazide, and adriamycin (ADR), respectively. [b] The values were calculated from the peak area ratio determined by ^{1}H NMR between poly(ethylene glycol) and benzyl groups of the PBLA block. [c] The numbers of hydrazide groups and ADR were determined by ^{1}H NMR and reversed-phase liquid chromatography (RPLC), respectively. [d] Polydispersity was measured for PEG−PBLA and Fol−PEG−PBLA to ensure the purity of starting materials.

Table 2. Particle Size and ζ Potential of the Micelles with Varying Folate Contents

	folate conjugation[a] (%)							
	0 (MA)	1 (FMA1)	2 (FMA2)	5 (FMA5)	10 (FMA10)	25 (FMA25)	50 (FMA50)	100 (FMA100)
particle size[b] (nm)	64.21	65.34	63.79	68.35	69.22	72.51	77.47	91.29
polydispersity index (μ/Γ^2)	0.1018	0.0951	0.1096	0.1232	0.1318	0.1437	0.1661	0.1973
ζ potential (mV)	−0.39	0.11	−0.67	−1.07	−1.98	−2.33	−6.95	−9.25

[a] It was determined by the mixing ratio of folate-conjugated block copolymers to the block copolymers without folate conjugation. [b] The micelles were filter-sterilized using 0.45 μm filter units (Millex-HV, Millipore, Co., Ltd., U.S.A.) prior to the measurements.

In Vitro Cytotoxicity Assay. In order to determine in vitro cytotoxicity of the micelles, a human pharyngeal cancer cell line KB was incubated with FMA, MA, and free ADR in various concentrations, changing exposure time. Exponentially growing KB cells were seeded on a 96-well culture plate (2000 cells/well) and preincubated for 24 h, followed by coincubation with the samples. After 3 and 24 h, cell culture media were replaced with fresh media, and the cells were incubated further for additional 24 h. The number of viable cells was determined by CellTiter-Glo luminescent cell viability assay (n = 8) that provides a convenient, rapid, and sensitive procedure based on quantitation of ATP, which signals the presence of metabolically active cells (*28*).

Flow Cytometric (FCM) Analysis. Cellular uptake of the micelles was analyzed by an EPICS XL Flow Cytometry Systems (Beckman Coulter, U.S.A.) monitoring autofluorescence of ADR accumulated in the cell. KB cells were seeded on a 12-well culture plate (30 000 cells/well) and preincubated for 24 h, followed by coincubation with FMA, MA, and ADR (10 mg/mL) for 3 and 24 h. The cells were then washed three times with PBS, detached by trypsinization, spun down by centrifugation, and dispersed again in PBS for FCM analysis. Data were acquired and processed with the accompanying software (*EXPO 32*).

Surface Plasmon Resonance (SPR) Analysis. Interaction between FBP and the micelles was analyzed by surface plasmon resonance (SPR) measurements using BIAcore 3000 (Biacore, Sweden). FBP was immobilized on the surface of a sensor chip (3 ng/mm^2 of FBP per channel), following the procedures provided by the manufacturer. FBP binding effects of both FMA and MA were evaluated at a flow rate of 10 μL/min with a concentration of 200 μg/mL. The micelles were allowed to flow for 30 min, and all samples were tested by replacing sensor chips on which FBPs were newly immobilized.

Pharmacological Study. Tumor-bearing mice were prepared by transplanting KB cells on the abdominal region of CD-1 nude mice (female, 6-week-old, n = 6, Charles River, Japan). When the tumor volume reached 100 mm^3, the micelles and free ADR as control were intravenously injected in a volume of 0.1 mL/10 g body weight. The drug dose was 10 mg/kg for both free ADR and the micelles (ADR equivalent). After drug injection, the blood, tumor, and major organs (heart, kidney, liver, and spleen) were collected at 0.5, 1, 3, 6, 9, and 24 h, followed by HPLC analysis as previously reported (*19*). Briefly, plasma was separated from the blood, and the tissues were homogenized prior to the measurements. Daunorubicin (DAU) was added to the specimens as an internal standard in 2 μg/mL, depending on sample amount. 200 μL of 10 mM HCl solution was then added to the specimens to cleave drug conjugation, and 1 mL of 100 mM ammonia buffer (pH 9.0) was applied after 24 h incubation. 5 mL of $CHCl_3$/MeOH (2:1) mixed solution was also added to the solution, and ADR and DAU were extracted by vigorous vortexing at 25 °C for 15 min. The organic layer was collected using Pasteur pipets and evaporated at 40 °C after centrifugation (1900 g, 15 min, 4 °C). Dry drugs were redissolved in 100 μL of DMF and injected to RPLC equipped with a μ Bondasphere 5μ C4 300 column and a fluorescence detector (Ex 485 nm, Em 560 nm). The area under the curve of concentration (AUC) vs time was calculated by the trapezoidal rule with the time points of 0.5, 1, 3, 6, 9, and 24 h. The unit for AUC is defined as % dose/mL plasma × h or % dose/g organ × h for the blood or other tissues (tumor, kidney, liver, spleen, and heart), respectively.

Table 3. Time-Dependent Increase in Cytotoxicity and Cellular Uptake of the Micelles (n = 8)[a]

sample	exposure time (h)	IC_{50}[b] (μg/mL ± SD)	relative index[c]	cellular uptake[d] (%)
ADR	3	0.069 ⊥ 0.014	1.97	100.00
	24	0.035 ± 0.011	1	100.00
FMA100	3	0.172 ± 0.017	4.91	92.51
	24	0.041 ± 0.012	1.17	94.95
MA	3	N.D.[e]	N.D.[e]	40.20
	24	0.263 ± 0.013	7.51	82.05

[a] Data were obtained from the eight independent experiments using a human pharyngeal cancer cell KB. [b] IC_{50} means the inhibitory concentration of the drugs required for reducing 50% of cell proliferation. The drug concentration of the micelles was calculated with respect to free ADR equivalents. [c] Relative index means the ratio between the IC_{50} of free ADR after 24 h incubation and the samples. [d] Cellular uptake of the micelles was analyzed by flow cytometric analysis monitoring autofluorescence of ADR accumulated in the cell. [e] N.D. means not determined.

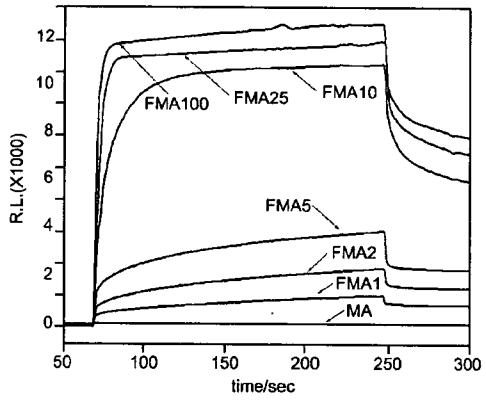

Figure 2. Surface plasmon resonance (SPR) analysis. FBP-binding selectivity of folate-conjugated micelles was evaluated by SPR measurements (eluent, 100 mM phosphate buffer; pH 7.4; flow rate, 10 mL/min; density of folate-binding protein, 3 ng/mm per channel; sample concentration, 200 μg/mL). Folate concentration on the surface of the micelles was varied to determine the optimum substitution rate.

In Vivo Antitumor Activity Evaluation. Tumor-bearing mice were prepared as described above. The micelles were injected from the tail vein three times with a four day interval in various doses (5, 10, 20, and 40 mg/kg). This administration schedule was based on the optimum regimen for free ADR as a control. However, free ADR was applied to the mice in limited doses (5, 10, and 15 mg/kg) due to the serious toxicity. Tumor growth and body weight of mice were checked at every second day. Tumor volume was calculated as volume $V = {}^1/_2 \times LW^2$, where the letters L and W denote the long and short diameters of the tumor tissue. Cancer treatment efficacy was analyzed by a treatment to control (T/C) ratio = $(V_c - V_t) \times 100/V_c$, where

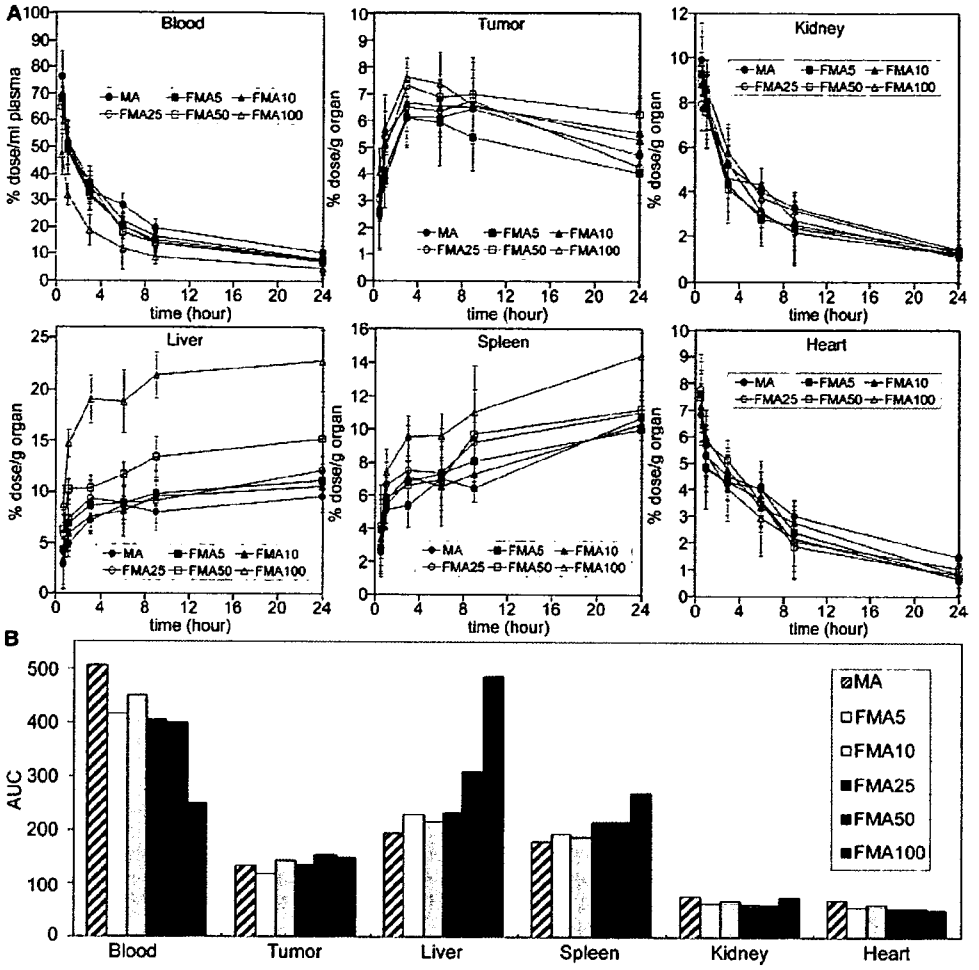

Figure 3. Pharmacokinetic profiles. Distribution of the micelles with varying folate amounts was measured in the blood compartment, tumor tissue, and major organs such as the liver, spleen, kidney, and heart (A). Experiments were carried out using tumor-bearing CD-1 nude mice (female, 6-week-old, $n = 6$) when the tumor volume reached 100 mm^3. Data are expressed as mean and mean ± SEM for relative and absolute values, respectively. Accumulation amounts for each micelle are compared in terms of the areas under the curve of concentration (AUC) vs time up to 24 h time period (B).

V_c and V_t are the mean tumor volumes of the control and the treated mice, respectively. The effective dose (ED) of each micelle was determined as the T/C ratio = 50, which means the average tumor volume of the mice decreased 50% of control values by drug treatments. The toxic dose (TD) was defined as the dose that causes 20% decrease in body weight of the mice after drug injection.

RESULTS AND DISCUSSION

Preparation of the Folate-Conjugated pH-Sensiive Polymeric Micelles (FMA). The molecular weight and composition distributions of self-assembling amphiphilic block copolymers, folate−poly(ethylene glycol)−poly(aspartate-hydrazone-adriamycin) [Fol−PEG−p(Asp-Hyd-ADR)] and α-methoxy-poly(ethylene glycol)−poly(aspartate-hydrazone-adriamycin) [PEG−p(Asp-Hyd-ADR)], were determined by GPC and ^{1}H NMR. Table 1 shows that these block copolymers were successfully prepared with a controlled number of hydrazide groups and ADR. It is noticeable that Fol−PEG−p(Asp-Hyd-ADR) block copolymers did not form any dimers or aggregates after folate conjugation. In addition, most notably, folate was functionalized only at γ-carboxylate position of its glutamate residue in this study by precision synthesis, as we previously reported elsewhere (*25*). This enables every folate molecule that is conjugated to the block copolymers to remain active, distinguishing our system from other folate conjugates. In many studies, folate molecules have been conjugated by using carbodiimide coupling reagents. The folate conjugated in this way is prone to making a mixture of α- and γ-carboxylate-functionalized forms. Because the α-carboxylate-functionalized form of folate loses its activity, the carbodiimide coupling method is substantially accompanied by the problems of undesirable introduction of inactive folate, which induces insufficient conjugation or incorrect quantification of active folate (*23, 24*). To the contrary, herein we can exclude the possibility that folate becomes inactive after conjugation, and therefore, it is able to clearly investigate the effects of folate conjugation on the biological properties of the micelles.

The particle size and ζ potential of the micelles were analyzed by Zetasizer Nano (Malvern, U.K.), and data are summarized in Table 2. Each micelle from Fol−PEG−p(Asp-Hyd-ADR) and PEG−p(Asp-Hyd-ADR) was abbreviated as FMA and MA, which denote folate micellar adriamycin and micellar adriamycin (without folate), respectively. The successive number after the abbreviated term of FMA in some descriptions indicates the mol % of Fol−PEG−p(Asp-Hyd-ADR) block copolymers in the micelles. For instance, FMA10 means that the micelles were prepared from 10% of Fol−PEG−p(Asp-Hyd-ADR) and 90% of PEG−p(Asp-Hyd-ADR) block copolymers. In all cases, the micelles exhibited particle sizes between 60 and 90 nm, while the distribution was narrow and monodisperse. Surface charge

of the micelles became negative, which is probably due to the carboxylic group remaining at the α-position of glutamate of the folate molecule. Although the micelle size slightly increased as folate concentration increased, these data demonstrate that the size and surface charge of the prepared micelles were still suitable for tumor-specific accumulation via the EPR effect after folate conjugation. When the micelle solutions were concentrated, however, aggregation between particles was observed in the case of FMA100. Such aggregation was able to be suppressed by decreasing the folate substitution ratio. Considering that MA (or FMA0) showed no aggregation during concentration, it is most probable that folate substitution increases the local concentration of folate molecules on the micelle surface, and thus, FMA aggregated due to the intermicellar hydrophobic interaction (*29*). Nevertheless, it must be noted that the micelles stably dispersed with 60−90 nm diameter up to 5 mg/mL concentration irrespective of folate substitution ratio. Because a high drug loading content (~30 wt %) is one of the characteristic advantages of the micelles, injecting the micelles above this concentration would not be realistic in terms of determining the injection dosage of ADR whose lethal dose ranges from 12.7 to 13.2 mg/kg. Therefore, it is concluded that the micelles with varying folate contents were stable at a size suitable for systemic drug delivery with sufficient drug concentration.

Folate Conjugation Significantly Increased in Vitro Cytotoxicity and Cellular Uptake of the Micelles. Table 3 shows a change in proliferation of KB cells treated by FMA100, MA, and free ADR and cellular uptake. It is of interest that the 50% inhibitory concentrations (IC_{50}) of cell growth decreased significantly in the case of the micelles by folate conjugation. Notably, cytotoxicity of FMA100 was as high as that of free ADR after 24 h incubation despite their different internalization mechanisms. In our previous studies, it is confirmed that this pH-sensitive micelle, which was designed to selectively release drugs in the intracellular region, requires relatively long exposure time sufficient for inhibiting cell growth (>10 h). It is because the micelles are required to enter the cell first and to release drug by sensing pH so that the released drugs accumulate in cell nuclei to intercalate with DNA, inducing cell death. In comparison with MA, FMA100 showed efficient cytotoxicity with a short exposure time of 3 h. These results suggest that folate conjugation promotes the interaction between the micelles and the cell. It is generally known that KB cells overexpress folate-binding proteins (FBPs) on the cell membrane, and therefore the FBPs can take up FMA100 to the cell interior efficiently via receptor-mediated endocytosis. Such enhanced cellular uptake probably induced higher cytotoxicity of FMA100 even with short exposure time. This hypothesis was also confirmed by flow cytometric analysis. As also summarized in Table 3, cellular uptake of FMA100 increased by folate conjugation, and such an increment corresponds well with enhanced cytotoxicity. Consequently, it is confirmed that folate conjugation enhanced cytotoxicity of the micelles by increasing cellular uptake and intracellular drug concentration.

FMA Recognized Folate-Binding Proteins (FBPs) Selectively and Strongly. Although in vitro cytotoxicity assay and flow cytometric analysis have proven that high efficacy of FMA was due to the increased intracellular drug concentration, the scientific evidence that elucidates the role of folate in accelerating cellular uptake was still required. In order to confirm the interaction between FMA and folate binding proteins (FBPs), we carried out surface plasmon resonance (SPR) analysis by using a sensor chip on which FBP molecules were immobilized. It is also of great importance to verify how folate concentrations affect FBP binding properties of the micelles, so we prepared FMA with varying folate substitution rates from 100% to 0%.

Table 4. Tumor-Specific Accumulation of the Micelles

sample	blood	tumor	liver	spleen	kidney	heart
AUC[a]						
MA	506.42	132.67	194.45	179.37	76.96	69.48
FMA5	415.53	117.13	229.35	193.65	63.15	57.01
FMA10	450.38	143.60	215.97	187.98	68.45	61.79
FMA25	405.17	135.48	233.33	215.24	61.58	55.59
FMA50	400.76	155.13	308.99	216.80	60.91	54.99
FMA100	250.16	147.86	487.30	270.14	76.10	51.87
			K_b value[b]			
MA	1	0.26	0.38	0.35	0.15	0.14
FMA5	1	0.28	0.55	0.47	0.16	0.15
FMA10	1	0.32	0.48	0.42	0.16	0.15
FMA25	1	0.33	0.58	0.53	0.17	0.16
FMA50	1	0.39	0.77	0.54	0.16	0.15
FMA100	1	0.59	1.95	1.08	0.30	0.25
			tumor to organ ratio[c] (AUC_{tumor}/AUC_{organ})			
MA	–	1	0.68	0.74	1.72	1.91
FMA5	–	1	0.51	0.60	1.81	1.92
FMA10	–	1	0.66	0.76	2.04	2.12
FMA25	–	1	0.58	0.63	1.94	2.16
FMA50	–	1	0.50	0.72	2.48	2.59
FMA100	–	1	0.30	0.55	1.94	2.41

[a] AUC denotes the area under a concentration curve that is obtained from the pharmacokinetic study with time points at 0.5, 1, 3, 6, 9, and 24 h. Values were calculated on the basis of the trapezoidal rule up to 24 h after intravenous injection. The unit for AUC is defined as % dose/mL plasma × h or % dose/g organ × h for the blood or other tissues (tumor, kidney, liver, spleen, and heart), respectively. [b] K_b value is defined as $[K_b = C_{tissue}/C_{blood}]$ where C_{tissue} and C_{blood} are the drug concentrations in the tissue and the blood, respectively. Each K_b value indicates distribution of the drugs in the vascular space ($K_b < 0.1$), extracellular space ($0.1 < K_b < 0.5$), and intracellular space ($0.5 < K_b$). [c] Tumor selectivity of the micelles was determined by calculating the relative accumulated concentrations between the tumor tissues and each organ (AUC_{tumor}/AUC_{organ}).

Figure 2 shows SPR signal intensity versus time for individual micelle samples. The micelles were flowed into the sensor channel for 3 min and rinsed with fresh buffer solution. The signal change indicates that FMA binds promptly and strongly to FBP in various folate contents while MA showed no interaction with FBP. Interestingly, FMA was able to recognize FBP even with 10% folate substitution ratio. However a significant decrease was found in the FBP binding effect between FMA10 and FMA5. In the meantime, the folate substitution rates can be converted from a percent to mol wt % on the basis of the molecular weight of block copolymers and the mixing ratio. It shows that 100% folate substitution ratio corresponds to 16.9 mmol wt % for a single micelle, and FMA10 and FMA5 were calculated to contain 1.7 and 0.8 mmol % of folate molecules, respectively. Therefore, these data revealed that the micelles require only a small quantity of folate to recognize FBPs. Folate is known to have a high affinity for FBP ($K_d < 1$ nM), and such high affinity seems to provide a strong binding property of FMA (*23, 24*).

Optimum Amounts of Folate-Facilitated Tumor Targeting Properties of the Micelles with Long Blood Circulation. The information regarding the relation between the amount of folate and biodistribution of the micelles is of primary importance to determining the compositions of FMA. Such compositions should be considered to maintain the balance between passive and active tumor targeting to realize an ultimate goal of drug delivery systems. For these reasons, we have investigated the biodistribution of FMA by changing folate contents. Figure 3 shows the distribution of the micelles in the blood compartment, tumor tissues, and major organs such as the liver, spleen, kidney, and heart after the intravenous injection. The area under a concentration curve (AUC) shows that the micelles circulated

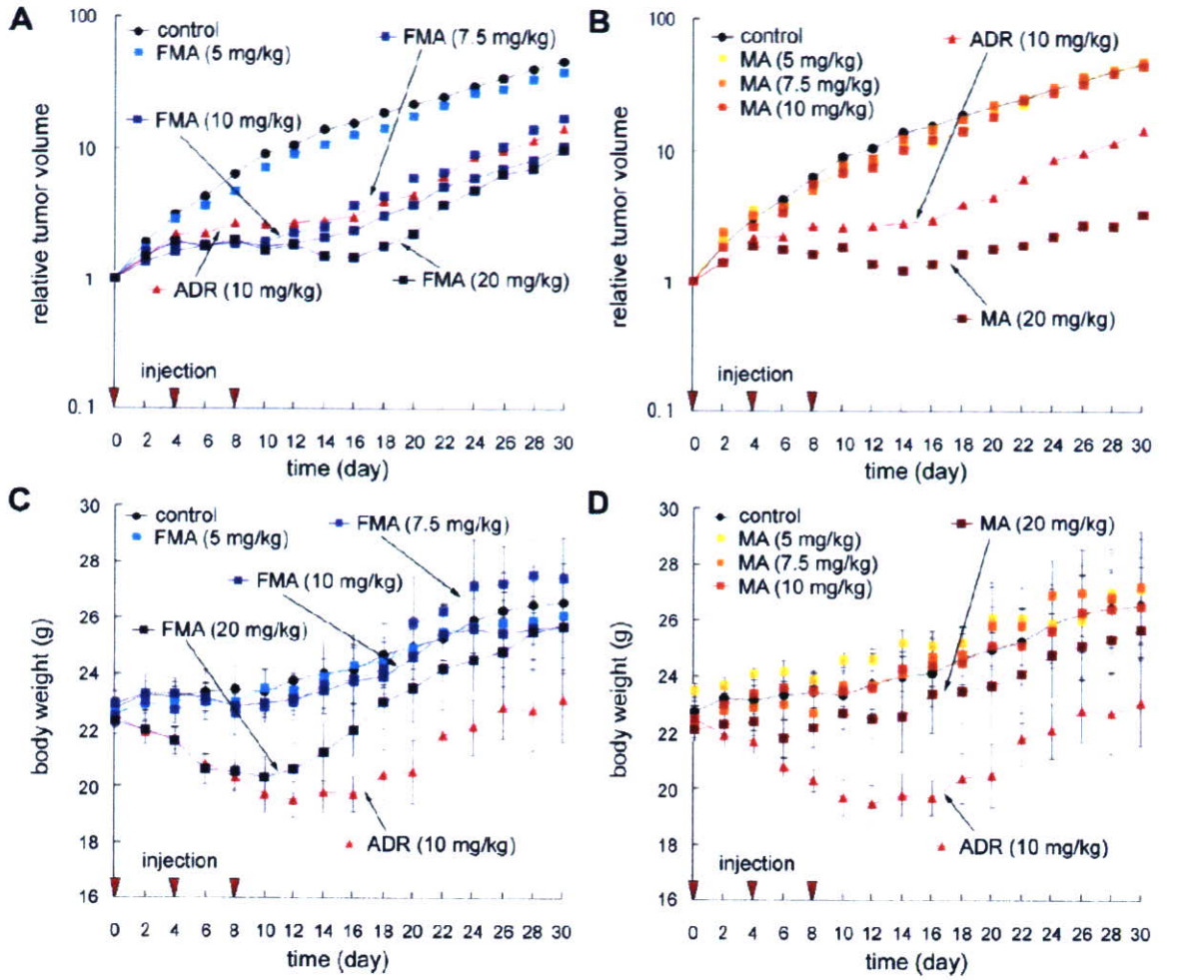

Figure 4. Tumor size and body weight change. The figure shows effective tumor-suppressing activity and low change in body weights over a broad range of injection doses of the folate-conjugated micelles (A and C). It clearly shows that the dose for effective tumor treatments decreased by folate conjugation compared to the micelles without folate, while toxicity remained lower than free drugs (B and D). Administrations were carried out 3 times with a 4 day interval into tumor-bearing CD-1 nude mice (female, 6-week-old, $n = 6$). The micelle doses are shown as ADR equivalents. Data are expressed as mean and mean ± SEM for relative and absolute values, respectively.

in the blood for a long time and their accumulation in tumor tissue increased significantly during the period of 24 h compared to normal organ. In the case of MA, the results correspond well with our previous data that revealed that the intracellular pH-sensitive micelles are characterized by prolonged circulation time in blood and tumor-specific accumulation (*19*). Such characteristic pharmacokinetic properties are considered to result from controlled drug release that can enhance the drug delivery efficiency of the micelles to the solid tumors. Regarding FMA, it is of interest that folate conjugation does not significantly affect the long-term circulation property of the micelles. FMA circulated in the blood for a prolonged time irrespective of folate content. However, the micelle accumulation in the liver as well as in the tumor changes obviously depending on the folate amount. As summarized in Table 4, a clear difference in tumor-specific accumulation was found between FMA and MA. The AUC values for each organ exhibit that FMA with a higher folate content showed a lower tumor-targeting property compared to MA. These results might be due to an increase in accumulation in the liver. Micelle accumulation in the liver was most probably due to the high FBP affinity of the micelles with increased folate concentration. In the meantime, the K_b values, which indicate the drug distribution within inter- and intracellular compartments, show that cellular uptake of FMA increased in tumor cells while remaining low in normal tissues. Nevertheless, the pharmacokinetic data also indicate that the possibility cannot be completely excluded that the micelles underwent nonspecific accumulation in normal organs after folate conjugation. It is not only because the K_b values increased, but also because the tumor to organ ratio (TOR) decreased as folate amounts increased. Accumulation in the liver increased, predominantly decreasing tumor-specific delivery efficiency. One of the previous studies showed that folate conjugation can induce higher hepatic clearance of the conjugates (*30*). Although expression of FBP in the liver would be suggested as a likely reason for the hepatic clearance, we considered that excessive conjugation of folate could increase accumulation of the micelles in normal organs. Therefore, it is concluded that the amount of folate should be carefully determined to facilitate tumor-targeting properties while maintaining long-term blood circulation. This would help us to minimize nonspecific distribution of the micelles in the body. Most noticeably, accumulation of the micelles in the tumor tissues did not significantly differ before and after folate conjugation in terms of pharmacokinetic profile. These findings indicate that the EPR effect seems to still be a major factor in determining the tumor accumulation of drug carriers for active targeting within a 24 h time range. In other words, folate conjugation would mainly affect the distribution of the micelles after extravasation rather than regulate migration of the micelles from the blood compartments to the tumor tissue.

FMA Showed Lower Toxicity and Higher Efficacy than Free Drug. The SPR analysis and biodistribution studies revealed that the optimum amount of folate conjugation is of significant importance to achieve passive and active drug targeting simultaneously. From the obtained data above, we selected FMA10 as the optimum micelle composition for further studies, which was believed to be the most suitable for the best performance in terms of tumor-specific drug delivery. In order to elucidate how folate affects in vivo antitumor activity of the micelles in detail, we have injected FMA, MA, and free ADR into the CD-1 nude mice implanted with human pharyngeal cancer KB cells by changing the dosage. Figure 4 show the changes in tumor size and body weight after drug administration. Free ADR was injected as a control, and it suppressed tumor growth at a dose of 10 mg/kg. The mice were also treated with different doses of free ADR, but there was no effect at 5 mg/kg. At a dose of 15 mg/kg, free ADR showed severe toxicity. These results indicated that free ADR was safe to exhibit the efficacy only within an extremely narrow dose range from 10 to 15 mg/kg. Indeed, body weight reduction was observed even at a dose of 10 mg/kg in the case of free ADR. In contrast to free ADR, MA was able to suppress tumor growth over a broad range of doses ranging from 20 to 40 mg/kg, while its toxicity was significantly low. Such effective and safe antitumor activity of the micelles was consistent with our previous results, which demonstrated the usefulness of intracellular pH-sensitive drug delivery (*18, 19*). Nevertheless, the effective dose (ED) of MA was relatively high compared to free ADR. In case of FMA, however, tumor growth was effectively suppressed with the same dose range of MA, but surprisingly, its ED decreased from 20 to 7.5 mg/kg while toxicity remained low. This value is even lower than the ED of free ADR (10 mg/kg), indicating that the micelles became more effective than free drug by folate conjugation. Therefore, these experimental data clearly elucidate that the drug carrier can show higher efficacy than free drug by optimally balancing passive and active tumor targeting properties as well as controlling drug release profile. It should be emphasized that, although the pharmacokinetic study showed that folate conjugation did not significantly improve the tumor-specific accumulation of the micelles, in vivo antitumor activity experiments clearly show that FMA is more effective to the cancer treatment than free ADR in terms of efficacy and safety. These results also support our hypothesis described above that active targeting seems to mainly affect the distribution profile of the drug carriers within the tumor tissues after extravasation rather than in the blood compartment. It is certain that more studies on this topic should be investigated further in the future. Nevertheless, it is of great importance that the ED of FMA decreased compared to free ADR as well as MA. A lowered dose is obviously beneficial for preventing possible long-term toxicity to the patients. From these aspects, it is concluded that our in vivo studies clearly demonstrate the effects of folate conjugation on active targeting drug delivery.

Folate Conjugation Decreased Effective Dose while Maintaining the Broad Therapeutic Window of the Micelles. The range of drug concentrations that provide the efficacy safely is known as the therapeutic window. If the injection dose is lower than this range, the drug cannot show its efficacy. To the contrary, if the injection dose is higher than the therapeutic window, the drug will induce either acute or chronic toxicity. In this study, animal studies have shown that FMA is more effective and safer than free drugs. In order to provide more objective criteria for evaluating efficacy of FMA, we analyzed antitumor activity of the micelles by calculating a treatment to control (T/C) ratio. Figure 5 exhibits the relation between the T/C ratio and a dosage. Each curve provides information about the tumor-suppressing efficacy of FMA, MA, and free ADR

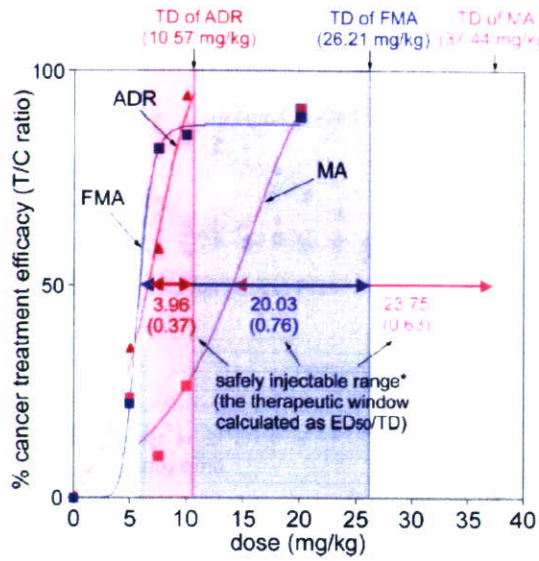

Figure 5. Treatment-to-control (T/C) ratio. Cancer treatment efficacy of the micelles was evaluated by comparing the therapeutic windows of FMA10, MA, and ADR, which were calculated from the ratio of ED_{50} to TD. ED_{50} and TD were defined as the effective dose that induces 50% decrease in tumor volume and the toxic dose that reduces 20% of body weight of mice, respectively. The data show the dose range in which each sample can be safely injected while achieving effective cancer treatments.

with respect to the control. Effective dose (ED) and toxic dose (TD) were defined as the doses that induce 50% of tumor growth (ED_{50}) and reduce 20% of body weight during the treatment, respectively. As drug concentrations increased, tumor growth suppression efficiency increased by all drug formulations. However, when we compare the effective doses, ED_{50} of free ADR is obviously close to its TD while ED_{50} of the micelles remained low compared to their TD. Namely, the safe dose of free ADR was only 3.96 mg/kg, but in contrast, FMA and MA were safely injectable between 20.03 and 23.75 mg/kg, respectively. These values correspond to 5.05- and 5.99-fold broader dose ranges than free drug. In particular, ED_{50} of FMA became lower than that of free ADR, and these results exemplify how active drug targeting is promising for cancer treatment. Most notably, such low toxicity and high efficacy were achieved by determining the optimum amount of folate on the micelle surface.

CONCLUSIONS

Integration of multiple functions into a single nanoparticle can broaden the possibilities of the macromolecular drug delivery systems for their future applications in the clinic. In this study, we have prepared a multifunctional polymeric micelle that is implemented with intracellular pH-dependent drug-releasing functionality and folate-mediated cancer cell targeting property simultaneously. By precision synthesis and preparation of the pH-sensitive micelles with varying folate contents, we were able to elucidate that the ligand-installed micelles for active drug targeting can be more effective than free drug in terms of antitumor activity, safety, pharmacokinetics, and bioavailability. It is of great interest that folate conjugation did not significantly improve the tumor accumulation of the micelles in the body because it induced a prominent increase in accumulation in the liver. However, when folate concentration was adjusted to achieve minimum ligand−receptor interaction, folate-conjugated micelles showed an effective cancer treatment efficiency that was even higher than free drugs as well as the micelles without folate conjugation. These findings clearly demonstrated that the

balance between passive and active drug targeting should be carefully considered to maximize the drug delivery efficiency as well as cytotoxic activity of the polymeric drug carriers.

ACKNOWLEDGMENT

The authors wish to express their thanks for the Project on the Materials Development for Innovative Nano-Drug Delivery Systems from the Ministry of Education, Culture, Sports, Science and Technology (MEXT), Japan.

LITERATURE CITED

(1) Duncan, R. (2006) Polymer conjugates as anticancer nanomedicines. *Nat. Rev. Cancer 6*, 688−701.

(2) Low, P. S., and Antony, A. C. (2004) Folate receptor-targeted drugs for cancer and inflammatory diseases. *Adv. Drug Delivery Rev. 56*, 1055−1058.

(3) Allen, T. M. (2002) Ligand-targeted therapeutics in anticancer therapy. *Nat. Rev. Drug Discovery 2*, 750−763.

(4) Lee, E. S., Na, K., and Bae, Y. H. (2005) Doxorubicin loaded pH-sensitive polymeric micelles for reversal of resistant MCF-7 tumor. *J. Controlled Release 103*, 405−418.

(5) Xu, Z., Gu, W., Huang, J., Sui, H., Zhou, Z., Yang, Y., Yan, Z., and Li, Y. (2005) In vitro and in vivo evaluation of actively targetable nanoparticle for paclitaxel delivery. *Int. J. Pharm. 288*, 361−368.

(6) Oyewumia, M. O., Yokela, R. A., Jaya, M., Coakleyb, T., and Mumper, R. J. (2004) Comparison of cell uptake, biodistribution, and tumor retention of folate-coated and PEG-coated gadolinium nanoparticles in tumor-bearing mice. *J. Controlled Release 95*, 613−626.

(7) Gabizon, A., Horowitz, A. T., Goren, D., Tzemach, D., Shmeeda, H., and Zalipsky, S. (2003) In vivo fate of folate-targeted polyethyleneglycol liposomes in tumor-bearing mice. *Clin. Cancer Res. 9*, 6551−6559.

(8) Jain, R. K. (1998) Delivery of molecular and cellular medicine to solid tumors. *J. Controlled Release 53*, 49−67.

(9) Matsumura, Y., and Maeda, H. (1986) A new concept for macromolecular therapeutics in cancer chemotherapy: mechanism of tumoritropic accumulation of proteins and the antitumor agent Smancs. *Cancer Res. 46*, 6387−6392.

(10) Maeda, H. (2001) SMANCS and polymer-conjugated macromolecular drugs advantages in cancer chemotherapy. *Adv. Drug Delivery Rev. 46*, 169−185.

(11) Minchinton, A. I., and Tannock, I. F. (2006) Drug penetration in solid tumours. *Nat. Rev. Cancer 6*, 583−592.

(12) Kamb, A. (2005) What's wrong with our cancer models? *Nat. Rev. Drug Discovery 4*, 161−165.

(13) Atkins, J. H., and Gershell, L. J. (2002) Selective anticancer drugs. *Nat. Rev. Cancer 1*, 645−646.

(14) Kataoka, K., Harada, A., and Nagasaki, Y. (2001) Block copolymer micelles for drug delivery: design, characterization and biological significance. *Adv. Drug Delivery Rev. 47*, 113−131.

(15) Nishiyama, N., and Kataoka, K. (2006) Nanostructured devices based on block copolymer assemblies for drug delivery: designing structures for enhanced drug function. *Adv. Polym. Sci. 193*, 67−101.

(16) Nishiyama, N., Bae, Y., Miyata, K., Fukushima, S., and Kataoka, K. (2005) Smart polymeric micelles for gene and drug delivery. *Drug Discovery Today: Technol. 2*, 21−26.

(17) Lavasanifar, A., Samuel, J., and Kwon, G. S. (2002) Poly(ethylene oxide)-block poly(L-amino acid) micelles for drug delivery. *Adv. Drug Delivery Rev. 54*, 169−190.

(18) Bae, Y., Fukushima, S., Harada, A., and Kataoka, K. (2003) Design of environment-sensitive supramolecular assemblies for intracellular drug delivery: polymeric micelles that are responsive to intracellular pH change. *Angew. Chem., Int. Ed. 42*, 4640−4643.

(19) Bae, Y., Nishiyama, N., Fukushima, S., Koyama, H., Matsumura, Y., and Kataoka, K. (2005) Preparation and biological characterization of polymeric micelle drug carriers with intracellular pH-triggered drug release property: tumor permeability, controlled subcellular drug distribution, and enhanced in vivo antitumor efficacy. *Bioconjugate Chem. 16*, 122−130.

(20) Mantovani, L. T., Miotti, S., Menard, S., Canevari, S., Raspagliesi, F., Bottini, C., Bottero, F., and Colnaghi, M. I. (1994) Folate binding protein distribution in normal tissues and biological fluids from ovarian carcinoma patients as detected by the monoclonal antibodies MOv18 and MOv19. *Eur. J. Cancer 30A*, 363−369.

(21) Weitman, S. D., Lark, R. H., Coney, L. R., Fort, D. W., Frasca, V., Zurawski, V. R., Jr., and Kamen, B. A. (1992) Distribution of the folate receptor GP38 in normal and malignant cell lines and tissues. *Cancer Res. 52*, 3396−3401.

(22) Hooijberg, J. H., de Vries, N. A., Kaspers, G. J. L., Pieters, R., Jansen, G., and Peters, G. J. (2005) Multidrug resistance proteins and folate supplementation: therapeutic implications for antifolates and other classes of drugs in cancer treatment. *Cancer Chemother. Pharmacol. 58*, 1−12.

(23) Leamon, C. P., and Reddy, J. A. (2004) Folate-targeted chemotherapy. *Adv. Drug Delivery Rev. 56*, 1127−1141.

(24) Lee, R. J., and Low, P. S. (1994) Delivery of liposomes into cultured KB cells via folate receptor-mediated endocytosis. *J. Biol. Chem. 269*, 3198−3204.

(25) Bae, Y., Jang, W.-D., Nishiyama, N., Fukushima, S., and Kataoka, K. (2005) Multifunctional polymeric micelles with folate-mediated cancer cell targeting and pH-triggered drug releasing properties for active intracellular drug delivery. *Mol. BioSyst. 1*, 242−250.

(26) Akiyama, Y., Nagasaki, Y., and Kataoka, K. (2004) Synthesis of heterotelechelic poly(ethylene glycol) derivatives having α-benzaldehyde and ω-pyridyl disulfide groups by ring opening polymerization of ethylene oxide using 4-(diethoxymethyl)benzyl alkoxide as a novel initiator. *Bioconjugate Chem. 15*, 424−427.

(27) Luo, J., Smith, M. D., Lantrip, D. A., Wang, S., and Fuchs, P. L. (1997) Efficient synthesis of pyrofolic acid and pteroyl A azide, reagents for the production of carboxyl differentiated derivatives of folic acid. *J. Am. Chem. Soc. 119*, 10004−10013.

(28) Crouch, S. P., Kozlowski, R., Slater, K. J., and Fletcher, J. (1993) The use of ATP bioluminescence as a measure of cell proliferation and cytotoxicity. *J. Immunol. Methods 160*, 81−88.

(29) Kanie, K., Nishii, M., Yasuda, T., Taki, T., Ujiieb, S., and Kato, T. (2001) Self-assembly of thermotropic liquid-crystalline folic acid derivatives: hydrogen-bonded complexes forming layers and columns. *J. Mater. Chem. 11*, 2875−2886.

(30) Shinoda, T., Takagi, A., Maeda, A., Kagatani, S., Konno, Y., and Hashida, M. (1998) In vivo fate of folate-BSA in non-tumor- and tumor-bearing mice. *J. Pharm. Sci. 87*, 1521−1526.

BC060401P

Colloidal Au Replacement Assay for Highly Sensitive Quantification of Low Molecular Weight Analytes by Surface Plasmon Resonance

Seiji Takae,[†] Yoshitsugu Akiyama,[†] Yuichi Yamasaki,[†,‡] Yukio Nagasaki,[§] and Kazunori Kataoka*[,†,‡,∥]

Department of Materials Engineering, Graduate School of Engineering, The University of Tokyo, 7-3-1 Hongo, Bunkyo-ku, Tokyo 113-8656, Japan, Center for NanoBio Integration, The University of Tokyo, 7-3-1 Hongo, Bunkyo-ku, Tokyo 113-0033, Japan, Tsukuba Research Center for Interdisciplinary Materials Science, Tsukuba University, Tennoudai 1-1-1, Tsukuba 305-8573, Japan, and Center for Disease Biology and Integrative Medicine, Graduate School of Medicine, The University of Tokyo, 7-3-1 Hongo, Bunkyo-ku, Tokyo 113-0033, Japan. Received November 9, 2006; Revised Manuscript Received April 16, 2007

A novel sensing method based on surface plasmon resonance (SPR) was developed for the highly sensitive quantification of low molecular weight (LMW) analytes (colloidal Au replacement assay). Gold nanoparticles (diameter = 20 nm) functionalized with lactosyl-poly(ethylene glycol) (PEG) were prepared and were specifically adsorbed onto a *Ricinus communis* agglutinin (RCA_{120})-immobilized SPR sensor chip surface. Subsequent injection of free D-galactose elicited the elution of the preadsorbed lactosyl-PEGylated gold nanoparticles in a manner proportional to the galactose concentration, achieving a substantial and quantitative analysis over a wide range of galactose concentrations (0.1−50 ppm). This method of D-galactose sensing through the substituted elution of preadsorbed nanoparticles from the sensor chip surface would be applicable for the highly sensitive SPR quantification of various LMW analytes, which are known to be difficult to detect by the conventional SPR sensing regime.

1. INTRODUCTION

The surface plasmon resonance (SPR) technique has been widely used in the real-time assay of biomolecular interactions (*1*−*4*). SPR is based on a change in the reflection of laser light from a metal−liquid surface, induced by a variation in the dielectric constant due to the adsorption of analyte molecules. Because this change is extremely sensitive and is correlated with the amount of adsorbed analytes, quantitative experiments with SPR are feasible for the monitoring of various biomacromolecules, including proteins, carbohydrates, and nucleic acid compounds. Nevertheless, the sensing of low molecular weight (LMW) compounds by SPR is generally difficult, mainly due to the inherently low response of analytes with a limited mass. An available method for the amplification of the SPR signal is the augmentation of the apparent mass of the analyte molecules. In this regard, gold nanoparticles modified with analytes were employed for the enhancement of the SPR signal (*5*−*7*). The amplification mechanisms of colloidal Au enhanced SPR are (i) the increased apparent mass of the analytes immobilized on gold nanoparticles and (ii) a coupling of the localized surface plasmon of gold nanoparticles with the propagating plasmon on the SPR gold surface. The colloidal Au enhanced SPR achieved the highly sensitive detection of the antigen−antibody interaction and DNA hybridization (*5*, *6*), but, as far as we know, this has not been applied to a direct quantitative assay of low molecular weight (LMW) analytes in sample solutions.

We now report a novel SPR method for the quantitative assay of LMW analytes (colloidal Au replacement assay) based on the elution of preadsorbed gold nanoparticles on the sensor chip surface induced by the injection of LMW analytes. In this method, it is crucial to minimize the nonspecific adsorption between the gold nanoparticles and the sensor chip surface. PEGylated gold nanoparticles possessing lactose moieties, as a ligand, at the distal end were then prepared by covering the nanoparticle with a densely tethered layer of a thiolated heterobifunctional PEG (*8*). Note that the hydrophilic PEG layer with a strong steric-repulsive property serves to minimize the nonspecific adsorption and agglomeration of gold nanoparticles in an aqueous medium (*9*). Eventually, the highly sensitive quantification of the label-free LMW compound, galactose, by SPR was achieved by monitoring the competitive elution of the lactosyl-PEGylated gold nanoparticles from a *Ricinus communis* agglutinin (RCA_{120}; a bivalent galactose-binding lectin)-immobilized sensor chip upon the injection of the sample solution containing a definite concentration of free galactose.

2. EXPERIMENTAL PROCEDURES

2.1. Materials. Gold nanoparticles (diameter = 20 nm) were purchased from British Biocell International (Cardiff, U.K.). Bovine serum albumin (BSA), lactosyl-albumin (lac-BSA), and NA3 glycan ($[Gal\text{-}GlcNAc]_3\text{-}Man_3\text{-}GlcNAc_2$, FW = 2006) were purchased from the Sigma-Aldrich Co. (St. Louis, MO). *Ricinus communis* agglutinin (RCA_{120}) was purchased from the Honen Co. (Tokyo, Japan). D-Galactose was purchased from Wako Pure Chemical Industries, Ltd. (Osaka, Japan). The CM3 sensor chip, acetate buffer (pH 5.5), and amine coupling kit were purchased from Biacore AB (Uppsala, Sweden). All reagents were used as received. The phosphate buffered saline (PBS, 150 mM, pH 7.4) was prepared using Dulbecco's PBS from the Dainippon-Sumitomo Pharma Co. (Osaka, Japan). Water was purified using a Milli-Q instrument (Millipore, Bedford, MA).

2.2 Preparation of PEGylated Gold Nanoparticles Possessing Varying Lactose Functionalities. PEGylated gold nanoparticles with varying lactose functionalities on the surface

* To whom correspondence should be addressed. Telephone: +81-3-5841-7138. Fax: +81-3-5841-7139. E-mail: kataoka@bmw.t.u-tokyo.ac.jp.

[†] Graduate School of Engineering, The University of Tokyo.

[‡] Center for NanoBio Integration, The University of Tokyo.

[§] Tsukuba University.

[∥] Graduate School of Medicine, The University of Tokyo.

10.1021/bc0603541 CCC: $37.00
Published on Web 06/19/2007

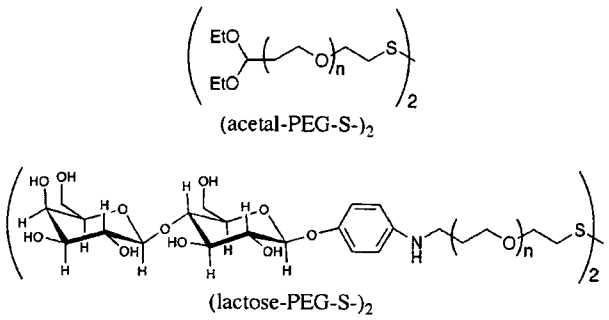

Figure 1. Chemical structures of (acetal-PEG-S-)$_2$ and (lactose-PEG-S-)$_2$.

were fabricated as previously reported (*10*). Briefly, a mixture of (acetal-PEG-S-)$_2$ (M_n = 12 100, Figure 1) and (lactose-PEG-S-)$_2$ (M_n = 12 200, Figure 1; the lactose functionality is 50%) of different molar ratios was added to the gold nanoparticle (diameter = 20 nm) solution (pH = 6.5) at room temperature. Lactose content on the gold nanoparticles was regulated by varying the feed molar ratio of (lactose-PEG-S-)$_2$ with (acetal-PEG-S-)$_2$ in the reaction mixtures. Since the reactivity of the disulfide group toward the surface of gold nanoparticles is likely to be equal between (lactose-PEG-S-)$_2$ and (acetal-PEG-S-)$_2$ because of their identical molecular weight with only a subtle change in the chain ends, the ratio of the lactose moieties on the gold surface is assumed to be equal to the feed ratio. Accordingly, the mol % of (lactose-PEG-S-)$_2$ in the feed was utilized to express the lactose functionalities (the fraction of tethered PEG having a lactosyl ligand at the distal end) on the PEGylated gold nanoparticles. Here, PEGylated gold nanoparticles with 0%, 25%, and 50% functionalities were prepared and abbreviated as lac0, lac25, and lac50, respectively. After 15 h of stirring, repetitive centrifugation and redispersion were carried out twice to remove any excess polymer from the solution. Finally, the nanoparticles were resuspended in PBS containing 0.01 wt % bovine serum albumin (BSA). The final concentration of the resuspended PEGylated gold nanoparticles was calculated from the absorbance at 523 nm using a UV−visible spectrophotometer (V-550 UV/vis spectrophotometer, JASCO, Japan). The calibration curve was prepared on the basis of the absorbance of the bare gold nanoparticles, because the UV−visible spectra revealed no substantial change even after the PEGylation of the gold nanoparticles (Supporting Information Figure S1).

2.3. Surface Plasmon Resonance Measurements. The SPR experiments were done using a Biacore 3000 instrument (Biacore AB, Uppsala, Sweden). RCA_{120} was immobilized on the surface of a CM3 carboxymethyl-dextran sensor chip using an amine coupling kit and 20 μg/mL RCA_{120} in 10 mM acetate buffer (pH 5.5) at the rate of 10 μL/min. Namely, carboxyl groups on the chip surface were activated by a mixture of succinimide (NHS) and carbodiimide (EDC) to form active esters, which then spontaneously react with the amino groups of RCA_{120}. Subsequently, excess ethanolamine was injected to deactivate the remaining active esters. The amount of the immobilized RCA_{120} was 1500 resonance units (RU) in all the experiments. A 0.1° SPR angle shift corresponds to 1000 RU, which is calibrated to be ca. 1 ng/mm^2, as provided by the manufacturer (Biacore) (*11*). Given that the molecular weight of RCA_{120} is ~120 000, it follows that 1500 RU = 1500 pg/mm^2 = 1.25×10^{-14} mol/mm^2 = 7.52×10^9 proteins/mm^2 = 7.52×10^{-3} proteins/nm^2. A similar procedure was carried out for a reference flow cell, for which the RCA_{120} injection is replaced with a blank injection of the buffer.

The lactosyl-PEGylated gold nanoparticles were then continuously injected over the flow cell modified with RCA_{120} and the unmodified flow cell at 25 °C. PBS containing 0.01 wt % BSA was used as the running buffer. All the data were obtained by signal subtraction of the blank flow cell injection from the RCA_{120}-immobilized flow cell, in order to remove any adverse contribution from the refractive index noise due to the bulk contribution of the sample injection. To assess the kinetic parameters, a global analysis of six concentrations of samples was performed using a 1:1 Langmuir model and bivalent model by *Biaevaluation 3.1* software.

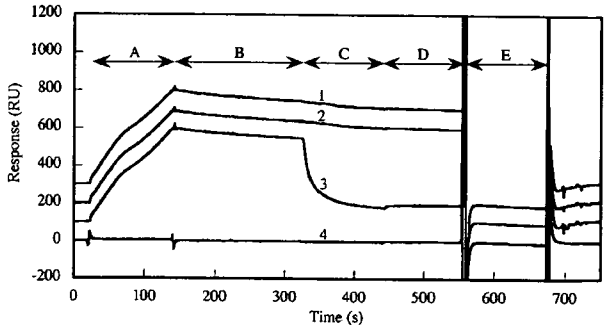

Figure 2. Sensorgrams for the interaction of PEGylated gold nanoparticles with RCA_{120} immobilized on the CM3 sensor chip. (region A): Injection of lac50 (lines 1−3) and lac0 (line 4). (region B): Flowing of running buffer (lines 1−4). (region C): Injection of running buffer (lines 1, 4), 100 μg/mL of glucose solution (line 2), and 100 μg/mL of galactose solution (line 3). (region D): Flowing of running buffer (lines 1−4). (region E): Injection of excess galactose (100 mg/mL, lines 1−4). All of these experiments were carried out at the flow rate of 5 μL/min.

2.4. Colloidal Au Replacement Assay. Lac25 and lac50 (15 nM and 5.2 nM particle concentrations, respectively) were injected over 1500 RU of an RCA_{120}-immobilized sensor chip at 10 μL/min for 5 and 3 min, respectively, producing a 900−1300 RU increase in the response. Subsequently, 0−100 ppm of galactose was injected for 5 min to elute the preadsorbed gold nanoparticles. In the elution sensorgram, the response level was normalized by the amount of the preadsorbed PEGylated gold nanoparticles (*12*, *13*). The dissociation rate constant (k_d) of the galactose-induced dissociation of lac25 and lac50 was calculated by a separate fitting against the first 15 s of the dissociation curves using a Langmuir model of the *Biaevaluation 3.1* software.

3. RESULTS AND DISCUSSION

3.1. Specificity of the Binding. Injection of lac50 (15 nM particle concentration) onto an RCA_{120}-immobilized CM3 sensor chip induced an obvious increase in the SPR signal (ca. 500 RU), in which lac0 was used as the control and conveyed low response (region A, Figure 2). The subsequent injection of 100 μg/mL galactose allowed a fast dissociation of the adsorbing lac50, whereas the same concentration of glucose did not trigger such a dissociation, and almost the same curve as the sensorgram recorded under the buffer injection was observed (region C, Figure 2), indicating the specific interaction of RCA_{120} with the lactose moieties on the PEGylated gold nanoparticles. The injection of a large excess of galactose (100 mg/mL) to the lac50-adsorbed sensor chip allowed the complete dissociation of the lac50, and eventually led to a regeneration of the sensor chip (region E, Figure 2).

3.2. SPR Response of PEGylated Gold Nanoparticles with Varying Lactose Surface Densities. Figure 3 shows the signal changes induced by the injection of the gold nanoparticles possessing various lactose densities (lac25, lac50) into a flow cell equipped with an RCA_{120}-immobilized sensor chip. Data for lac-BSA and NA3 glycan are also shown as controls. Obviously, the lactose-functionalized gold nanoparticles displayed a much higher response compared to the controls,

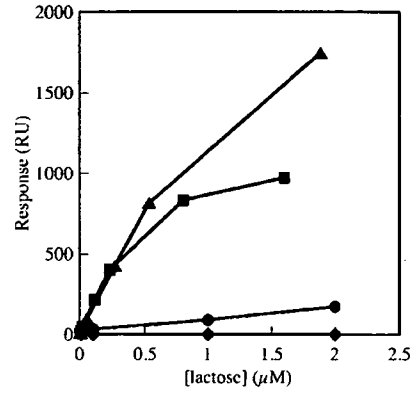

Figure 3. Binding response of various lactosylated substances onto an RCA_{120}-immobilized CM3 sensor chip (square, lac25; triangle, lac50; circle, lac-BSA; diamond, NA3 glycan). The samples were injected for 10 min at the flow rate of 5 μL/min.

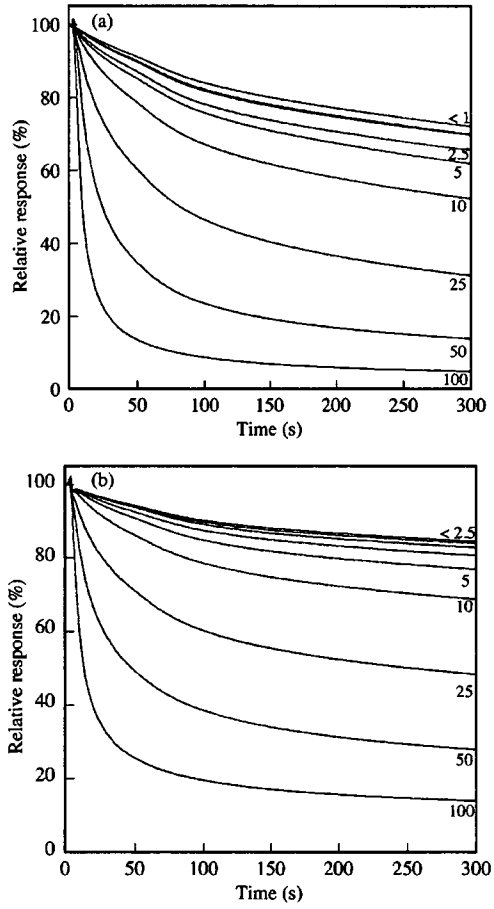

Figure 4. The elution profiles of preadsorbed lac25 (a) and lac50 (b) from an RCA_{120}-immobilized CM3 sensor chip induced by the injection of galactose. Lac25 and lac50 were injected over the sensor chip at the flow rate of 10 μL/min for 5 and 3 min, respectively. The elution of the preadsorbed nanoparticles was done by the injection of 0.1−100 ppm of galactose for 5 min. The magnitude of the net response increase from the baseline at the beginning of the elution phase was taken as 100% for each sensorgram for data normalization. The values indicated in each of the sensorgrams represent the injected galactose concentration (ppm).

indicating that the enhancement of the SPR signal based on the gold nanoparticles effectively worked. This is considered to be due to the large apparent mass and the coupling effect between the gold nanoparticles and gold surface on the sensor chip (*5*, *6*). Interestingly, the lac50 system revealed a more effective signal enhancement than the lac25 system at the same lactose concentration, even where the former has a particle concentration that is half of the latter, suggesting that the former has a higher binding affinity to the immobilized RCA_{120} than the latter.

Table 1. Kinetic Parameters for lac25-RCA_{120} and lac50-RCA_{120} Systems Determined from SPR Analysis

sample	k_a ($M^{-1}s^{-1}$)	k_d (s^{-1})	K_D (M)	χ^2
lac25	1.56×10^5	9.88×10^{-4}	6.34×10^{-9}	1.21
lac50	2.41×10^5	4.97×10^{-4}	2.06×10^{-9}	3.88

3.3. Kinetic Evaluations. To quantitatively assess the affinity of lac25 and lac50 to RCA_{120}, a kinetic analysis was carried out. A series of different concentrations of the samples was injected at the flow rate of 20 μL/min for 2 min, followed by the flowing of running buffer for 5 min to observe the dissociation phase of the samples (Figures S2 and S3). As shown in Table 1, the equilibrium dissociation constants (K_D) of the lac25-RCA_{120} and lac50-RCA_{120} systems were calculated to be 6.34×10^{-9} and 2.06×10^{-9} M, respectively, using global fitting of a Langmuir model. On the other hand, the K_D of a single lactose molecule with RCA_{120} was reported to be 3.7×10^{-3} M (*14*). It is notable that the lactosyl gold nanoparticles-RCA_{120} system has a K_D that is 6 orders smaller than the lactose-RCA_{120} system. In our previous report, lactose-installed polymeric micelles behave as a multivalent ligand for an RCA_{120}-immobilized sensor chip with a decrease in the K_D of the same order of magnitude as this system with respect to a monovalent interaction (*15*). Considering this previous report of multivalent interactions and several other references about multivalent glyconanoparticles (*16*, *17*), all of which showed that multivalency causes the nonlinear increase in the affinity, it is reasonable to also assume in this case the multivalent interactions: multiple lactose ligands on a single particle would bind with several lectin molecules on a sensor chip. In fact, in the global fitting of the sensorgrams of lac25 and lac50 using a bivalent model, a sufficiently low χ^2, a measure of the accuracy of the fitting, was obtained (1.26 and 4.03, respectively), making this fit acceptable by Biacore standards ($\chi^2 < 10$).

To gain insight into the multivalent interaction of lactose molecules on the gold nanoparticles with RCA_{120} on the sensor chip, the inter-lactose distance on the gold nanoparticles as well as the distance between two RCA_{120} molecules on the sensor chip were calculated on the basis of the following three assumptions; (i) uniform distribution of lactose molecules on the gold nanoparticles as well as of RCA_{120} molecules on the sensor chip, (ii) reduced apparent valency of an immobilized RCA_{120} molecule on the sensor chip from bivalent to monovalent against lactose molecules on the gold nanoparticles due to a steric restriction, and (iii) all of the lactose ligands accessible to the binding site of RCA_{120}, neglecting the possible decrease in the number of available lactose molecules due to the concealment of the chain end into the flexible PEG coils. As previously reported (*10*), the diameter including the PEG layer of the PEGylated gold nanoparticles was evaluated to be 33.3 nm from SEM, and the number of PEG chains on a single gold nanoparticle was estimated to be 520 chains/particle from a thermogravimetric analysis. Accordingly, the number of lactose molecules and the inter-lactose distance on lac25 and lac50 were calculated and summarized in Table 2 . Alternatively, on the basis of the RCA_{120} density described in the Experimental Section 2.3 (7.52×10^{-3} proteins/nm^2), the area occupied by a single RCA_{120} molecule on the sensor chip was calculated to be $(7.52 \times 10^{-3})^{-1} = 133$ nm^2/protein. Consequently, the average distance between RCA_{120} on the sensor chip surface is approximated to be $133^{0.5} = 11.5$ nm. It may be reasonable to then assume at least a bivalent interaction, because the inter-lactose distance on lac25 and lac50 is calculated to be less than